PACIFIC EARTHQUAKE ENGINEERING RESEARCH CENTER

Towards Deep Learning-Based Structural Response Prediction and Ground Motion Reconstruction

Khalid M. Mosalam

Issac K.T. Pang

Selim Günay

Department of Civil and Environmental Engineering
University of California, Berkeley

PEER Report No. 2025/01
Pacific Earthquake Engineering Research Center
Headquarters at the University of California, Berkeley
January 2025

PEER 2025/01
January 2025

Towards Deep Learning-Based Structural Response Prediction and Ground Motion Reconstruction

Khalid M. Mosalam

Issac K.T. Pang

Selim Günay

Department of Civil and Environmental Engineering
University of California, Berkeley

PEER Report No. 2025/01

Pacific Earthquake Engineering Research Center
Headquarters, University of California, Berkeley
January 2025

ABSTRACT

This research presents a novel methodology that uses Temporal Convolutional Networks (TCNs), a state-of-the-art deep learning architecture, for predicting the time history of structural responses to seismic events. By leveraging accelerometer data from instrumented buildings, the proposed approach complements traditional structural analysis models, offering a computationally efficient alternative to nonlinear time history analysis.

The methodology is validated across a broad spectrum of structural scenarios, including buildings with pronounced higher-mode effects and those exhibiting both linear and nonlinear dynamic behaviors. Applications demonstrate high prediction accuracy across diverse building types, using datasets from the California Strong Motion Instrumentation Program (CSMIP). Training dataset development is grounded in core principles of structural dynamics, with results interpreted through the lens of earthquake engineering. Additionally, a pilot study is presented to reconstruct ground motions using the measured responses of a building.

Despite recognizing limitations such as dataset size and model generalizability, the study highlights the transformative potential of advanced Artificial Intelligence (AI) techniques in seismic response prediction. Future research will investigate complementary strategies, including physics-informed AI, transformer architectures, and neural operators, to further enhance prediction accuracy. These advancements pave the way for improved Structural Health Monitoring (SHM) and support the evolution of Performance-Based Earthquake Engineering (PBEE) methodologies.

Keywords: Deep Learning; Ground Motion Reconstruction; Structural Health Monitoring; Structural Response Prediction; Temporal Convolutional Networks.

ACKNOWLEDGMENTS

The authors sincerely acknowledge California Strong Motion Instrumentation Program (CSMIP) for providing the accelerometer data used in this study. Their invaluable contributions have significantly advanced research in structural response analysis and ground motion prediction.

Special thanks are extended to the staff of the Pacific Earthquake Engineering Research (PEER) Center at the University of California, Berkeley, for their continued guidance and support. The facilities and resources provided by the PEER Labs were instrumental in conducting laboratory experiments and validating the developed models.

The authors gratefully recognize the funding agencies that made this research possible. This study was initially supported by the California Department of Conservation, California Geological Survey, through Strong Motion Instrumentation Program Agreement No. 1022-002 for the project entitled "Structural Response Prediction Using Deep Neural Networks," which provided critical financial resources to launch this work. Additional support following the conclusion of this funding was provided by the Taisei Chair in Civil Engineering at the University of California, Berkeley, a contribution that is deeply appreciated.

The opinions, findings, conclusions, and recommendations expressed in this publication are those of the authors and do not necessarily reflect the view of California Department of Conservation, California Geological Survey, Pacific Earthquake Engineering Research (PEER) Center, or the Regents of the University of California.

CONTENTS

LIST OF TABLES

LIST OF FIGURES

1 Introduction

Earthquakes pose a significant risk to the built environment, making accurate prediction of structural responses an essential aspect of earthquake engineering. Over the years, researchers and engineers have developed various methodologies to assess the seismic performance of structures, ranging from physical experimentation to computational modeling. These methods aim to understand how structures respond to seismic loads, detect potential vulnerabilities, and ultimately enhance the resilience of the built environment. However, traditional approaches often face limitations related to cost, scalability, or computational intensity, necessitating innovative solutions.

This study introduces a novel approach that combines advanced deep learning techniques with principles of structural dynamics to address these challenges. Specifically, it leverages Temporal Convolutional Networks (TCNs), a state-of-the-art deep learning architecture, to predict the time history of structural responses caused by earthquakes. By integrating data-driven methodologies with engineering knowledge, the study aims to enhance predictive accuracy and provide practical tools for seismic performance assessment. The following sections of this chapter outline the motivation for the research, define its objectives, and describe the scope of the study. A summary of the organization of the report is also provided.

1.1 MOTIVATION

Structural response prediction is a cornerstone of earthquake engineering. It allows engineers to evaluate how structures will perform under seismic loads, enabling safety and reliability. Historically, three primary methods have been used to determine the dynamic structural responses:

1. **Field Instrumentation**: Installing sensors on real structures provides direct and realistic measurements of their behavior. However, this approach is limited by the relatively small number of instrumented buildings worldwide.

2. **Laboratory Testing**: Physical models, such as those tested on shaking tables or in quasi-static setups, offer detailed insights into the dynamic response. While valuable, these tests are often constrained by high cost, time requirements, and limited scalability.

3. **Numerical Modeling**: Computational simulations are widely accessible and flexible, making them the most common approach. However, they rely heavily on assumptions about

material behavior, boundary conditions, and loading, which can reduce their accuracy compared to real-world observations.

Recent advancements in Artificial Intelligence (AI) and deep learning offer an opportunity to address these limitations. TCNs are particularly promising, as they can analyze sequential data to learn temporal patterns, providing a computationally efficient alternative to traditional nonlinear time history analysis. This study builds on these developments, applying TCN to predict the structural responses across a variety of scenarios, including both linear and nonlinear behavior.

1.2 OBJECTIVES

This research aims to bridge the gap between data-driven methodologies and structural engineering principles, improving the accuracy and applicability of AI techniques in earthquake engineering. The specific objectives are:

1. **Develop a Methodology**: Create a robust framework for predicting the time history of structural responses during seismic events using TCNs.
2. **Test Across Diverse Scenarios**: Apply the methodology to a wide range of cases, including buildings with higher mode effects and both linear and nonlinear responses, to evaluate the accuracy of TCN predictions.
3. **Solve an Inverse Problem**: Investigate the potential of TCNs to address the inverse problem of predicting ground motion from structural response data.
4. **Integrate Structural Dynamics**: Combine AI techniques with fundamental principles of structural dynamics and earthquake engineering to enhance the interpretability and physical validity of predictions.

By achieving these objectives, this research seeks to provide a computationally efficient complement –or even alternative– to traditional nonlinear time history analysis.

1.3 SCOPE

There has been limited research on using deep learning techniques to predict the complete time history of structural responses. While some studies focus on predicting peak response [24], the entire response history offers a more comprehensive understanding of the structural behavior. This is particularly important for applications like Structural Health Monitoring (SHM), where the peak response is often insufficient for identifying the existence, severity, and location of damage [17, 18, 19].

Existing studies have explored machine learning approaches to predict the structural responses [4, 23, 12, 14]. However, they typically focus on specific structural components or individual instrumented buildings or bridges. These studies often lack detailed physical interpretations of the predictions. This research addresses these gaps by applying TCNs to predict the time history of the structural responses across a variety of systems. The characteristics of these systems, outlined in Table 1.1, include elastic and inelastic behaviors, single-mode and higher-modes effects, and varying damping ratios. Inverse problem solutions are also explored to predict ground motions from structural response data.

Table 1.1: Features characterizing the earthquake response of different structural systems.

<table>
<tr><th>Response</th><th>System</th><th>Feature 1</th><th>Feature 2</th><th>Feature 3</th></tr>
<tr><td rowspan="3">Linear elastic</td><td>SDOF</td><td>Natural period</td><td>Damping ratio</td><td rowspan="3">Ground motion</td></tr>
<tr><td>Low- & Mid-rise Buildings</td><td>First mode period</td><td>Varying first mode damping ratios</td></tr>
<tr><td>Tall Buildings</td><td>Periods for multiple modes</td><td>Damping ratios of multiple modes</td></tr>
<tr><td rowspan="2">Inelastic</td><td>SDOF</td><td>Natural period damping ratio</td><td>Force capacity</td><td rowspan="2">Ground motion</td></tr>
<tr><td>Low & Mid-rise Buildings</td><td>Elongation of first mode period</td><td>Varying first mode damping ratio</td></tr>
</table>

1.4 ORGANIZATION OF THE REPORT

The report structure ensures a logical flow, guiding the reader through the methodology, applications, and implications of the research. It is organized into seven chapters:

1. **Chapter 1** introduces the motivation, objectives, and scope of the study, providing the foundation for the research.

2. **Chapter 2** details the development of the TCN methodology, including its theoretical framework and architecture. It also discusses related foundational architectures like Recurrent Neural Networks (RNN), Long Short-Term Memory (LSTM) networks, and Convolutional Neural Networks (CNNs).

3. **Chapters 3, 4 & 5** focus on specific applications of the TCN method, addressing linear elastic response predictions, inelastic response modeling, and ground motion predictions, respectively.

4. **Chapter 6** provides a comprehensive summary of the results, draws conclusions, and discusses their significance.

5. **Chapter 7** concludes the report by highlighting limitations and suggesting potential directions for future research.

2 Methodology

Analyzing structural responses as time series at various locations is crucial for understanding the impacts of severe earthquakes. Traditionally, nonlinear structural responses under seismic events have been evaluated using computational models such as the Finite Element Method (FEM) based on mechanics and physics principles. However, these methods are computationally intensive, requiring step-by-step time integration using numerical techniques (e.g., via the Newmark β method) and nonlinear iterative solutions (e.g., the Newton-Raphson method) at each time step. This computational demand becomes particularly challenging when dealing with large-scale analyses, such as regional seismic damage assessments, or when rapid results are needed for critical decision-making. Consequently, there is a pressing need for faster, more efficient approaches to predict structural responses at key locations.

In recent years, Long Short-Term Memory (LSTM) networks have gained significant attention for their ability to predict structural responses [23]. Most studies have relied on standard or "vanilla" LSTM networks configured to handle sequential data. However, recent advancements have explored integrating LSTM networks with additional components, such as convolution layers and attention mechanisms, to improve task-specific performance and prediction accuracy. These enhanced architectures provide better modeling of nonlinear and complex dependencies in time-series data.

Another promising approach is the transformer architecture, which has demonstrated exceptional performance in modeling global dependencies across sequential data in domains like Natural Language Processing (NLP) [22]. Despite its success in other fields, the application of transformers to structural dynamics remains limited. The quadratic computational complexity of Transformers with respect to sequence length poses a significant challenge, particularly for high-resolution ground motion and corresponding structural response data, which is common in earthquake engineering. This complexity can lead to prohibitive computational costs, making transformers less practical for real-time decision-making or large-scale analyses where efficiency is paramount.

For this study, we have adopted the Temporal Convolutional Network (TCN) as the primary model for predicting structural responses. TCNs have shown superior accuracy and computational efficiency compared to other models, particularly for time-series data. They are well-suited for capturing long-term dependencies and offer significant advantages in training and prediction speed. These features make TCN an ideal choice for the objectives of the study.

To provide a comprehensive understanding of the TCN model, this chapter also reviews the following foundational methods traditionally used for sequential data processing:

1. **Recurrent Neural Networks (RNN)**: Introduced as one of the earliest neural network architectures for sequential data, RNNs are designed to process sequences by maintaining a hidden state that evolves with each time step. However, RNNs suffer from *vanishing gradient problems*, which limit their effectiveness for long sequences.

2. **Long Short-Term Memory (LSTM) Networks**: LSTMs address the limitations of RNNs by introducing memory cells and gating mechanisms that enable better handling of long-term dependencies in data. These features made LSTMs a popular choice for structural response prediction.

3. **Convolutional Neural Networks (CNNs)**: Originally developed for image processing [16], CNNs have been adapted for temporal data. By applying convolutional operations, CNNs efficiently capture local patterns in data, but they struggle with long-term dependencies without significant adaptation.

TCN builds upon the principles of CNNs, adapting them for temporal data using *causal and dilated convolutions*[1]. These adaptations allow TCN to model sequential dependencies effectively, offering faster computation and scalability compared to RNNs and transformers. By leveraging the strengths of TCN, this study aims to advance predictive capabilities for structural response analysis, providing an efficient and scalable alternative to traditional computational methods.

2.1 DEEP LEARNING IN STRUCTURAL RESPONSE PREDICTION

Deep Learning (DL) has become a powerful tool for predicting structural response to dynamic loading, such as earthquakes. By leveraging its capacity to model complex, nonlinear relationships, DL provides a robust framework to establish the connection between input ground motion data and output structural responses. This section outlines the theoretical framework and mathematical foundations of using DL in this context.

2.1.1 Problem Formulation

Predicting the structural responses involves mapping the input ground motion data:

$$\mathbf{X} = \{\mathbf{x}_1, \mathbf{x}_2, \ldots, \mathbf{x}_i, \ldots, \mathbf{x}_N\}$$

[1] A *causal convolution* ensures that the output at a given time step depends only on the current and previous input time steps, preventing any “future” information from influencing the prediction. This is crucial for time-series tasks where the prediction at a specific time must not have access to future values in the sequence. A *dilated convolution* is also known as “atrous convolution”, where the word *atrous* is derived from Latin and French to mean *hole*. It is a convolutional operation where the filter is applied to the input with gaps (dilations) between the sampled input points. This allows the convolution to capture a larger receptive (i.e., more context) without increasing the number of parameters or computational cost significantly.

to the output structural response data:

$$\mathbf{Y} = \{\mathbf{y}_1, \mathbf{y}_2, \ldots, \mathbf{y}_i, \ldots, \mathbf{y}_N\},$$

where N denotes the total number of time steps. The input features may include ground motion acceleration or velocity at a specific point in time, and the structural responses, may represent quantities such as floor accelerations or displacements, or story drifts. It is to be noted that the index i represents the component of the vector.

The goal is to find a function $f_{\boldsymbol{\theta}}$ that minimizes the discrepancy between the predicted responses $\hat{\mathbf{Y}} = f_{\boldsymbol{\theta}}(\mathbf{X})$ and the actual responses $\mathbf{Y}$. This is formulated as an optimization problem:

$$\boldsymbol{\theta}^* = \arg\min_{\boldsymbol{\theta}} \mathcal{L}\left(f_{\boldsymbol{\theta}}(\mathbf{X}), \mathbf{Y}\right), \tag{2.1}$$

where $\mathcal{L}$ is a loss function that quantifies prediction errors. Common loss functions include:

- **Mean Squared Error (MSE)**:

$$\mathcal{L}_{\text{MSE}} = \frac{1}{N}\sum_{i=1}^{N}(\mathbf{y}_i - \hat{\mathbf{y}}_i)^2, \tag{2.2}$$

- **Mean Absolute Error (MAE)**:

$$\mathcal{L}_{\text{MAE}} = \frac{1}{N}\sum_{i=1}^{N}|\mathbf{y}_i - \hat{\mathbf{y}}_i|. \tag{2.3}$$

2.1.2 Deep Learning Framework

DL models are composed of multiple layers that sequentially transform the input data into predictions. The relationship between inputs and outputs is expressed as[2]:

$$\hat{\mathbf{y}}_i = f_{\boldsymbol{\theta}}\left(\mathbf{x}_i\right) = f^{(L)}\left(f^{(L-1)}\left(\ldots f^{(1)}\left(\mathbf{x}_i\right)\right)\right), \tag{2.4}$$

where $f^{(l)}$ represents the operation of the l-th layer, such as a linear transformation or an activation function, where $l \in \{1, 2, \ldots, L-1\}$.

2.1.3 Key Components of Deep Learning Models

1. Linear Transformation where each layer computes a weighted sum of its inputs as follows:

$$\mathbf{z}^{(l)} = \mathbf{W}^{(l)}\mathbf{a}^{(l-1)} + \mathbf{b}^{(l)}, \tag{2.5}$$

where $\mathbf{W}^{(l)}$ and $\mathbf{b}^{(l)}$ are the weights and biases of the l-th layer, and $\mathbf{a}^{(l-1)}$ represents the outputs of the previous layer. This equation is a general description applicable to all intermediate layers of the network.

[2] Eq. 2.4 is a general representation of the deep learning framework. The time-dependence nature of some specific deep learning architecture is explained in a Section 2.5.

2. Nonlinear Activation Function where nonlinearity is introduced through activation functions, enabling the model to capture complex relationships:

$$\mathbf{a}^{(l)} = \phi(\mathbf{z}^{(l)}), \tag{2.6}$$

where ϕ is the activation function, e.g., $ReLU(z) = \max(0, z)$, or other nonlinear functions.

3. Output Layer where the final layer L is distinct from the preceding layers in its purpose—it produces the model's predictions. For a regression task, the prediction is computed as:

$$\hat{\mathbf{y}}_i = \mathbf{W}^{(L)}\mathbf{a}^{(L-1)} + \mathbf{b}^{(L)}, \tag{2.7}$$

where $\mathbf{W}^{(L)}$ and $\mathbf{b}^{(L)}$ are the weights and biases of the output layer, and $\mathbf{a}^{(L-1)}$ represents the outputs of the last hidden layer. Unlike earlier layers, which primarily extract and transform features, the output layer is specifically tailored to generate task-specific outputs, such as predictions in regression or probabilities in classification.

2.1.4 Training and Optimization

Training a DL model involves optimizing its parameters, $\boldsymbol{\theta} = \{\mathbf{W}^{(l)}, \mathbf{b}^{(l)}\}_{l=1}^{L}$, to minimize the loss $\mathcal{L}$. This is typically performed through gradient-based methods such as *stochastic gradient descent* (SGD):

$$\boldsymbol{\theta}^{(l+1)} = \boldsymbol{\theta}^{(l)} - \alpha \nabla_{\boldsymbol{\theta}} \mathcal{L}, \tag{2.8}$$

where α is the *learning rate*, and $\nabla_{\boldsymbol{\theta}} \mathcal{L}$ represents the gradient of the loss function with respect to the model parameters.

2.1.5 Evaluation Metrics

To assess the performance of the trained model, several quantitative and qualitative metrics are used. These metrics are discussed in the following paragraphs:

1. **Correlation Coefficient**: Measures the linear correlation between predicted and actual responses:

$$R = \frac{\sum_{i=1}^{N} (\mathbf{y}_i - \overline{\mathbf{y}})(\hat{\mathbf{y}}_i - \overline{\hat{\mathbf{y}}})}{\sqrt{\sum_{i=1}^{N} (\mathbf{y}_i - \overline{\mathbf{y}})^2 \sum_{i=1}^{N} (\hat{\mathbf{y}}_i - \overline{\hat{\mathbf{y}}})^2}}, \tag{2.9}$$

   where $\overline{\mathbf{y}}$ and $\overline{\hat{\mathbf{y}}}$ are the mean values of $\mathbf{y}_i$ and $\hat{\mathbf{y}}_i$, respectively. It is to be noted that the index i represents the component of $\mathbf{y}_i$.

2. **Error Distribution**: The relative error at each time step is calculated as:

$$e_i = \frac{\mathbf{y}_i - \hat{\mathbf{y}}_i}{\max_i(\mathbf{y}_i)}, \tag{2.10}$$

   where the normalization with $\max_i(\mathbf{y}_i)$ ensures comparability across different response types and levels.

3. **Visualization**: To ensure the model's practical utility and interpretability, its predictions, i.e., how well the model reproduces the underlying patterns and structural behavior, are also evaluated using visual overlays. This is conducted for:

    - *Time Domain*: The predicted responses are plotted against the actual responses over time to check for alignment and consistency in capturing dynamic trends.
    - *Frequency Domain*: The Fourier amplitude spectra of the predicted and actual responses are compared to ensure that the model captures key frequency components, such as the natural frequencies.

2.1.6 Summary

By combining DL's capacity to model complex relationships with comprehensive evaluation methods, e.g., quantitative metrics with qualitative visualizations, this approach offers a computationally efficient alternative to traditional methods. It allows for accurate prediction of structural responses under dynamic loads, paving the way for advancements in Structural Health Monitoring (SHM) and Earthquake Engineering.

2.2 RECURRENT NEURAL NETWORK

A Recurrent Neural Network (RNN) is a DL architecture designed for modeling sequential data. Unlike standard neural networks, RNN incorporates not only the current input but also information from previous steps, making it ideal for capturing temporal dependencies within data sequences. The core component of an RNN is the hidden state vector $\mathbf{h}_t$, which maintains information about all prior steps. This state enables RNN to understand context over time, such as words in a sentence or trends in time-series data.

The architecture of a basic RNN is depicted in Figure 2.1, where $\mathbf{x}_t$, $\mathbf{h}_t$, and $\mathbf{y}_t$ represent the input vector, hidden state vector, and output vector at time step t, respectively. The relationships governing RNN computations are:

$$\mathbf{h}_t = f(\mathbf{W}_{hh}\mathbf{h}_{t-1} + \mathbf{W}_{hx}\mathbf{x}_t + \mathbf{b}_h), \tag{2.11}$$

$$\mathbf{y}_t = f(\mathbf{W}_{yh}\mathbf{h}_t + \mathbf{b}_y), \tag{2.12}$$

where f is the activation function, $\mathbf{W}_{hh}$, $\mathbf{W}_{hx}$, and $\mathbf{W}_{yh}$ are weight matrices, and $\mathbf{b}_h$ and $\mathbf{b}_y$ are bias vectors.

While RNN is powerful, it suffers from a critical limitation: the vanishing gradient problem. This issue arises during training when backpropagated gradients diminish exponentially through time, making it challenging for the model to learn long-term dependencies. To address this, specialized RNN architectures such as Long Short-Term Memory (LSTM) were developed. These architectures use gating mechanisms to regulate the flow of information, enabling them to retain long-term dependencies effectively.

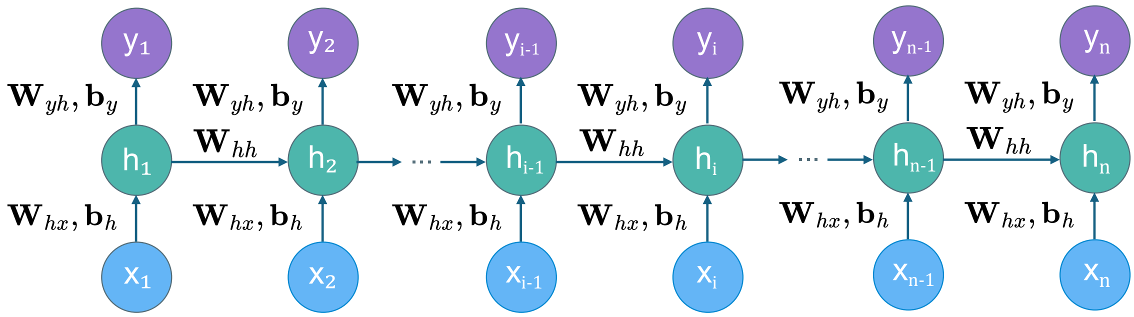

Figure 2.1: Simple RNN architecture.

RNN is designed to handle sequential data by maintaining a hidden state that evolves over time. The output at the final time step n can be expressed recursively, showcasing the dependency on all previous hidden states and inputs:

$$\mathbf{y}_n = g(\mathbf{W}_{yh} f(\mathbf{W}_{hh} \dots f(\mathbf{W}_{hh}\mathbf{h}_1 + \mathbf{W}_{hx}\mathbf{x}_2 + \mathbf{b}_h) \cdots + \mathbf{W}_{hx}\mathbf{x}_n + \mathbf{b}_h) + \mathbf{b}_y). \tag{2.13}$$

The RNN is trained by minimizing a loss function L, which measures the discrepancy between the predicted outputs $\hat{\mathbf{Y}} = \{\hat{\mathbf{y}}_1, \hat{\mathbf{y}}_2, \dots, \hat{\mathbf{y}}_N\}$ and the ground truth $\mathbf{Y} = \{\mathbf{y}_1, \mathbf{y}_2, \dots, \mathbf{y}_N\}$. Gradients are computed using Backpropagation Through Time (BPTT). The gradient of the loss with respect to the weights $\mathbf{W}$ is:

$$\frac{\partial L}{\partial \mathbf{W}} = \frac{\partial L}{\partial \mathbf{y}_n} \cdot \frac{\partial \mathbf{y}_n}{\partial \mathbf{h}_n} \prod_{t=2}^{n} \frac{\partial \mathbf{h}_t}{\partial \mathbf{h}_{t-1}} \cdot \frac{\partial \mathbf{h}_1}{\partial \mathbf{W}}. \tag{2.14}$$

A key challenge in training RNN is the vanishing gradient problem. The derivative of the hidden state at time t with respect to the previous hidden state $\mathbf{h}_{t-1}$ is:

$$\frac{\partial \mathbf{h}_t}{\partial \mathbf{h}_{t-1}} = f'(\mathbf{W}_{hh}\mathbf{h}_{t-1} + \mathbf{W}_{hx}\mathbf{x}_t + \mathbf{b}_h) \cdot \mathbf{W}_{hh}. \tag{2.15}$$

When the eigenvalues of W_{hh} or the derivative of the activation function f' are small, repeated multiplication causes the gradients to diminish exponentially. Conversely, large eigenvalues can lead to the exploding gradient problem. The mathematical model of RNN highlights their ability to capture temporal dependencies via recursive hidden state updates. However, challenges like vanishing and exploding gradients motivate the development of advanced architectures such as LSTM.

2.3 LONG SHORT TERM MEMORY

LSTM [10], Figure 2.2, is a type of RNN designed to address the vanishing gradient problem. By incorporating a memory cell and gating mechanisms, LSTM is capable of learning long-term dependencies in sequential data. The architecture of an LSTM includes three primary gates: the forget gate, which determines what information to discard; the input gate, which decides what new

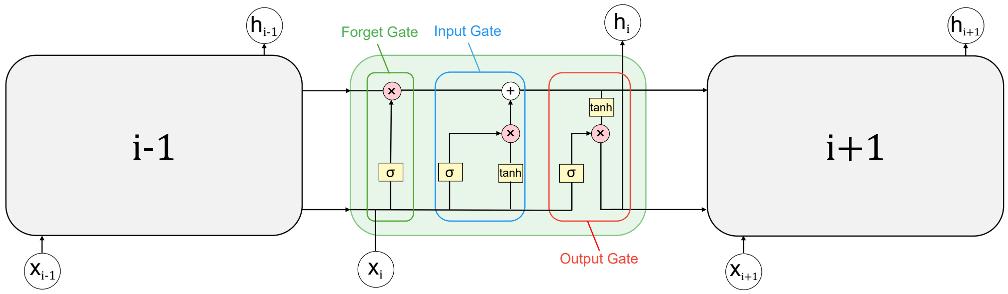

Figure 2.2: A typical LSTM cell configuration.

information to add; and the output gate, which controls what information is passed as the hidden state.

The defining feature of an LSTM is its cell state, denoted as c_t, which acts as a conveyor belt to preserve information across time steps. The gating mechanisms ensure selective retention or forgetting of information, enabling the model to overcome the gradient vanishing problem effectively. The LSTM cell operations at time step t are described by the following equations. The forget gate, responsible for deciding which information from the previous cell state should be discarded, is given by:

$$\mathbf{f}_t = \sigma(\mathbf{W}_{fx}\mathbf{x}_t + \mathbf{W}_{fh}\mathbf{h}_{t-1} + \mathbf{b}_f). \tag{2.16}$$

The input gate, which determines what new information to add to the cell state, is computed as:

$$\mathbf{i}_t = \sigma(\mathbf{W}_{ix}\mathbf{x}_t + \mathbf{W}_{ih}\mathbf{h}_{t-1} + \mathbf{b}_i), \tag{2.17}$$

The candidate cell state is:

$$\tilde{\mathbf{c}}_t = \tanh(\mathbf{W}_{cx}\mathbf{x}_t + \mathbf{W}_{ch}\mathbf{h}_{t-1} + \mathbf{b}_c). \tag{2.18}$$

The cell state is updated by combining the previous cell state $\mathbf{c}_{t-1}$, modulated by the forget gate, and the candidate cell state, scaled by the input gate:

$$\mathbf{c}_t = \mathbf{f}_t \odot \mathbf{c}_{t-1} + \mathbf{i}_t \odot \tilde{\mathbf{c}}_t, \tag{2.19}$$

where $\odot$ denotes element-wise multiplication.

The output gate determines which part of the cell state contributes to the hidden state:

$$\mathbf{o}_t = \sigma(\mathbf{W}_{ox}\mathbf{x}_t + \mathbf{W}_{oh}\mathbf{h}_{t-1} + \mathbf{b}_o), \tag{2.20}$$

The hidden state is calculated as:

$$\mathbf{h}_t = \mathbf{o}_t \odot \tanh(\mathbf{c}_t). \tag{2.21}$$

Here, $\mathbf{f}_t$, $\mathbf{i}_t$, $\mathbf{o}_t$, and $\tilde{\mathbf{c}}_t$ represent the forget gate, input gate, output gate, and candidate cell state, respectively. The terms $\mathbf{W}_{fx}, \mathbf{W}_{fh}, \mathbf{W}_{ix}, \mathbf{W}_{ih}, \mathbf{W}_{cx}, \mathbf{W}_{ch}, \mathbf{W}_{ox}, \mathbf{W}_{oh}$ are weight matrices, and $\mathbf{b}_f, \mathbf{b}_i, \mathbf{b}_c, \mathbf{b}_o$ are bias vectors. The activation functions σ (sigmoid) and $\tanh$ (hyperbolic tangent) provide nonlinearity.

LSTMs excel in capturing long-term dependencies in sequential data while mitigating the vanishing and exploding gradient problems. The memory cell allows information to flow unchanged across many time steps unless explicitly modified, making LSTMs particularly effective for tasks involving long sequences. LSTMs are widely used in various domains, including time series forecasting, anomaly detection, natural language processing (e.g., machine translation, text generation), speech recognition, and video analysis. These applications benefit from the LSTM's ability to model temporal and sequential dependencies effectively. By introducing memory cells and gating mechanisms, LSTMs provide a robust framework for handling sequential data. Their ability to selectively retain relevant information and mitigate the vanishing gradient problem makes them a foundational tool in modern deep learning. However, one significant drawback of LSTMs is their slow training process, which led us to adopt TCN as an alternative in this project. Since TCN is primarily built upon the principles of CNN, it is important to first introduce CNN.

2.4 CONVOLUTIONAL NEURAL NETWORK

Convolutional Neural Network (CNN) is a class of deep learning models designed to process data with spatial or sequential structure. While CNNs are widely known for their application in computer vision, their underlying principles —particularly convolutional operations (Figure 2.3)— make them highly versatile and applicable to other domains, including structural response prediction. In structural applications, sequential data such as ground motion time histories or vibration signals can be represented as one-dimensional arrays. CNNs can process this data by applying filters to capture local and global patterns, making them a powerful tool for time-series modeling.

The convolutional layers in CNN apply learnable filters to input data, extracting hierarchical features that progressively capture more complex patterns. For structural response prediction, this hierarchical feature extraction can be used to identify critical temporal patterns in seismic input data and structural responses, such as acceleration, velocity, or displacement. Additionally, CNN's ability to handle multi-channel input, such as data from multiple accelerometers, makes it particularly suitable for analyzing structural systems with multiple degrees of freedom.

Although CNNs were originally designed for spatial data, their principles have been extended to sequential data processing, as demonstrated in Temporal Convolutional Networks (TCN). TCN leverages CNN's convolutional capabilities while introducing causal and dilated convolutions to handle long-term dependencies and maintain temporal fidelity. These adaptations make CNN a foundational component in the development of TCN and its application to structural response prediction.

CNN introduces key improvements over traditional fully connected neural networks:

- **Local Connections**: Units in a CNN layer are connected to local patches of the previous layer through a set of weights called a filter or kernel. This contrasts with fully connected layers, where every neuron is connected to every neuron in the previous layer.
- **Shared Weights**: Filters are shared across all spatial locations in a layer, making CNNs computationally efficient and invariant to local translations in the input.

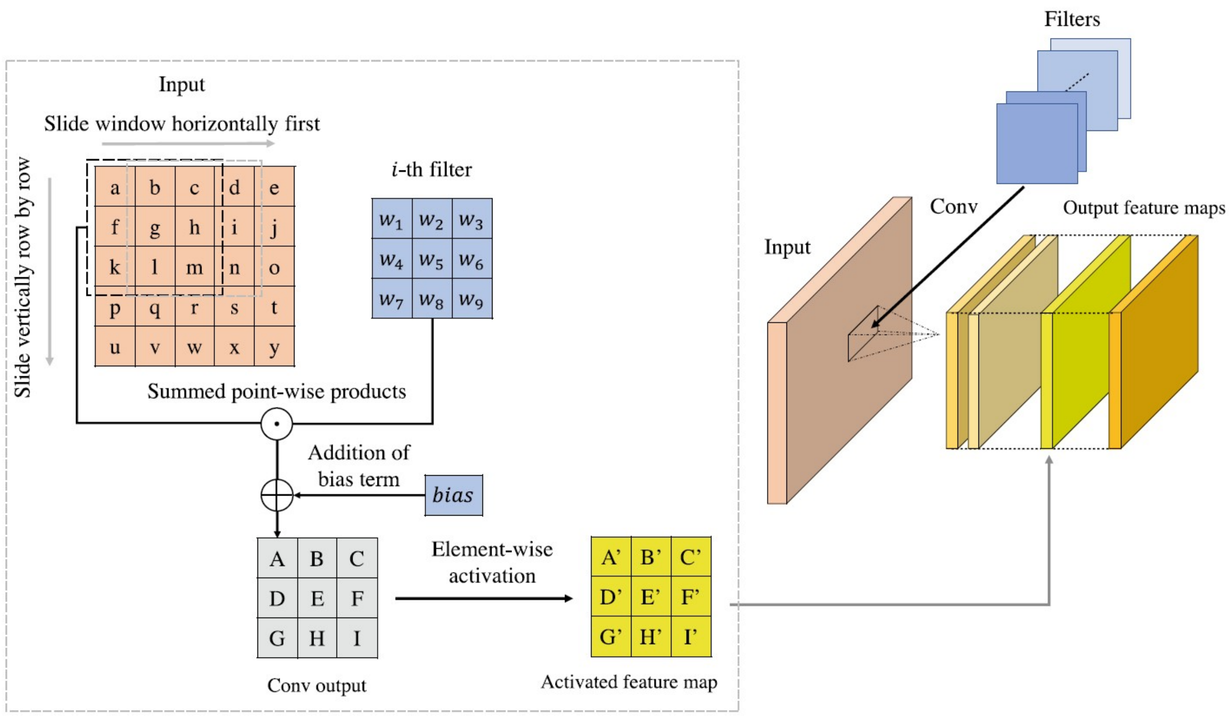

Figure 2.3: A typical convolutional operation [16].

- **Pooling**: Pooling layers downsample feature maps by summarizing the presence of features in a local patch. Max-pooling, for instance, retains the maximum value in a patch, reducing spatial dimensions and increasing robustness to small translations and distortions.
- **Multi-Layer Feature Extraction**: Lower layers in CNNs capture basic features like edges, while higher layers learn complex features like shapes and objects. This hierarchical feature extraction allows CNNs to identify patterns across multiple levels of abstraction.

The operation of a CNN layer involves a convolution between the input feature map and a filter, followed by the application of a non-linear activation function. Mathematically, the convolution operation for a single output feature map can be expressed as:

$$y_{i,j} = f\left(\sum_{m=1}^{M}\sum_{n=1}^{N} x_{i+m,j+n} \cdot w_{m,n} + b\right), \tag{2.22}$$

where $y_{i,j}$ is the output feature map at position (i, j), $x_{i+m,j+n}$ is the input value at position $(i + m, j + n)$, $w_{m,n}$ is the filter weight at position (m, n), b is the bias term, and f is the activation function (e.g., ReLU).

Pooling layers further reduce the spatial dimensions of the feature map. For max-pooling, the output is given by:

$$p_{i,j} = \max_{(m,n)\in\text{patch}} x_{i+m,j+n}, \tag{2.23}$$

where patch refers to the local region over which pooling is applied.

Despite its success in vision-based tasks, the use of CNN for time-series modeling in SHM remains limited. However, the underlying principles of convolution and pooling make CNN a valuable component for sequential data analysis, which is further extended in models like the Temporal Convolutional Network (TCN).

2.5 TEMPORAL CONVOLUTIONAL NETWORK

The TCN [13] is a deep learning architecture designed for sequence modeling and time-series prediction. By leveraging convolutional layers, TCN provides an efficient alternative to recurrent architectures such as Long Short-Term Memory (LSTM) networks, while maintaining the capability to model long-term dependencies. TCN is closely related to Convolutional Neural Network (CNN), adapting its convolutional principles to sequential data.

Temporal Convolutional Network (TCN) combines the strengths of convolutional and recurrent architectures by introducing several key characteristics. It employs causal convolutions, which ensure that predictions at time t depend only on data from time t and earlier, thereby preserving the temporal order of the sequence. Additionally, TCN utilizes dilated convolutions to extend the receptive field exponentially without increasing the depth of the network, enabling the efficient capture of long-term dependencies in the data. Unlike LSTM networks, TCN processes the entire input sequence in parallel, significantly improving training and inference times.

The core operation in TCN is the convolution applied to sequential data. For a 1D convolution, the output at time t for a single filter is:

$$y_t = \sum_{k=0}^{K-1} w_k \cdot x_{t-k} + b, \tag{2.24}$$

where y_t is the output at time t, x_{t-k} is the input at time $t-k$, w_k is the weight for the k-th position of the filter, K is the filter size (kernel size), and b is the bias term.

In TCN, this basic convolution is extended with dilations to capture dependencies across larger temporal ranges. Causal convolutions ensure that no future information is used when predicting the output at time t. This is achieved by zero-padding the input such that the convolutional operation respects the temporal order. The causality constraint is crucial for time-series tasks where predictions must depend only on past data.

TCN is built upon the principles of CNN by utilizing convolutional layers to extract hierarchical features. However, while CNN is typically used for spatial data like images, TCN modifies it for sequential data using causal and dilated convolutions. This makes TCN an efficient alternative to recurrent architectures like LSTM. Unlike LSTM, which processes data sequentially through time, TCN processes the entire input sequence in parallel, leveraging convolutional operations. This parallelism results in faster training and inference times. Additionally, while LSTM uses gates to control information flow, TCN employs the receptive field and stacked dilated convolutions to achieve similar capabilities.

Temporal Convolutional Network combines the strengths of CNN and LSTM, providing a powerful framework for sequential data modeling. By leveraging causal and dilated convolutions,

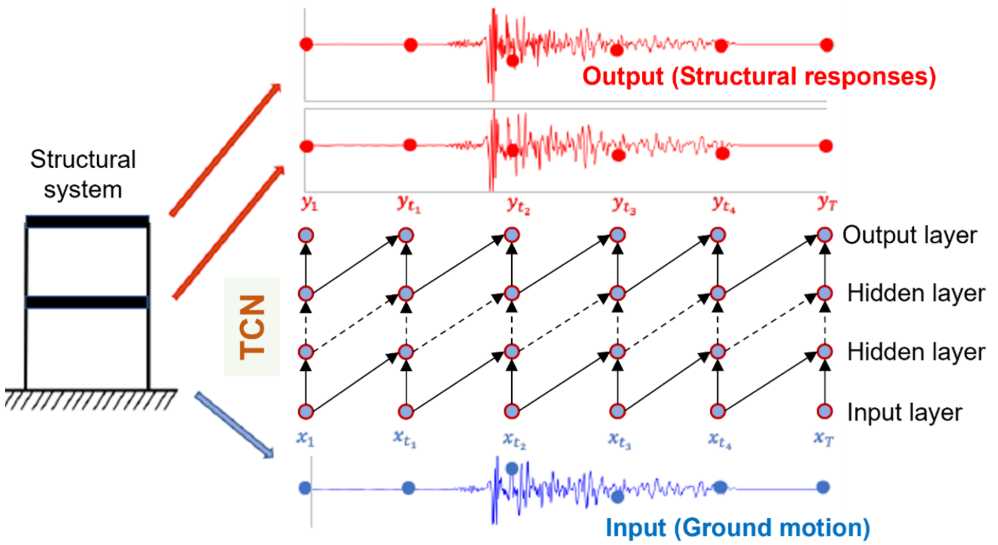

Figure 2.4: Schematic of TCN architecture applied to a two-story frame.

TCN achieves efficient parallel processing and robust long-term dependency modeling, making it a strong candidate for time-series prediction and other sequential tasks.

The architecture of Temporal Convolutional Networks (TCN) (Figure 2.4) makes it particularly well-suited for predicting structural responses under seismic events. Given input ground motion data, TCN predicts time-history responses such as acceleration, velocity, or displacement. For example, a TCN maps the input ground motion $\mathbf{x}(t)$ to the structural response $\mathbf{y}(t)$ as:

$$\mathbf{y}(t) = \mathcal{F}(\mathbf{x}(t)), \tag{2.25}$$

where $\mathcal{F}$ represents the learned mapping function.

In TCN, the input is processed to generate predictions for the structural response as output. The input and output structures are defined as:

$$\text{Input} = (n_{\text{events}}, n_{\text{steps}}, \text{features}_x) \quad \& \quad \text{Output} = (n_{\text{events}}, n_{\text{steps}}, \text{features}_y)\,, \tag{2.26}$$

where n_{events} represents the number of earthquake events, and n_{steps} is the maximum number of time steps across all events. Zero padding is applied to events with fewer time steps than n_{steps} to ensure consistency in input size. The terms features_x and features_y denote the input features (e.g., accelerometer data) and the predicted variables (e.g., acceleration, velocity, displacement), respectively. The timestep size is consistent across all events.

The fundamental operation of TCN is the causal convolution, which ensures that the output at time t depends only on inputs from the current and previous time steps, preserving temporal causality. The causal convolution is mathematically defined as:

$$y_t^{(l)} = \sum_{i=0}^{k-1} w_i^{(l)} \cdot x_{t-i\cdot d}, \tag{2.27}$$

where K is the kernel size, defining the number of input values considered, d is the dilation factor that spaces the kernel elements to cover long-range dependencies, $w_i^{(l)}$ are the weights of the convolutional filter at layer l, and $x_{t-i\cdot d}$ is the input at time $t - i \cdot d$.

The dilation factor d is adjusted to exponentially expand the receptive field with each layer, enabling TCN to efficiently capture dependencies over extended sequences without excessive computational cost. After the convolutional layers, the temporal information is aggregated through a fully connected layer to generate the final output. This operation is expressed as:

$$\hat{\mathbf{y}} = \mathbf{W} \cdot \mathbf{y}_{n_{\text{steps}}} + \mathbf{b}, \tag{2.28}$$

where $\hat{\mathbf{y}}$ is the final output prediction (a vector), $\mathbf{W}$ is the weight matrix of the fully connected layer, $\mathbf{b}$ is the bias vector, and $\mathbf{y}_{n_{\text{steps}}}$ is the output of the last timestep from the TCN. In this study, the configuration settings for the TCN are as follows:

- **Kernel size:** : 10
- **Number of filters:** 20
- **Number of epochs:** 200
- **Minimum learning rate:** 10^{-5}
- **Maximum dilation factor:** 512

TCNs offer several advantages for structural response prediction. One key advantage is their temporal fidelity, as causal convolutions preserve temporal causality, ensuring that predictions rely solely on past information. Additionally, dilated convolutions allow TCNs to efficiently model long-range dependencies without significantly increasing computational complexity, making the architecture computationally efficient. Furthermore, TCNs are highly scalable, capable of handling large-scale datasets effectively, which is essential for practical applications in structural response prediction.

TCNs face several challenges. A major limitation is their dependency on extensive labeled datasets, which are often required for accurate training and generalization across diverse scenarios. Another challenge lies in their interpretability; purely data-driven models such as TCNs may lack physical interpretability, which is critical for applications in structural engineering. This limitation can be addressed by integrating physics-informed neural networks (PINNs) to enhance the model's ability to incorporate domain knowledge and improve its physical consistency. Despite these limitations, TCNs provide a powerful framework for modeling complex temporal relationships in structural response prediction. Their unique combination of efficiency, scalability, and temporal accuracy makes them a promising tool for advancing Performance-Based Earthquake Engineering (PBEE) and SHM.

In the following chapters, we will leverage TCN to predict both linear and nonlinear structural responses, explore ground recovery dynamics, and address other critical tasks in structural response modeling. By applying TCN to these diverse challenges, we aim to demonstrate its versatility and effectiveness in solving real-world engineering problems. The used source codes will be made publicly available on GitHub at: https://github.com/STAIRlab/dyntrace.

3 Linear Elastic Response Prediction

Linear elastic response of systems with various characteristics, namely a Single-Degree-of-Freedom (SDOF) numerical model, instrumented low-rise buildings and instrumented tall buildings, are presented in this chapter. As shown in Table 1.1, the features that define the responses of these systems depend on different and varying number of dynamic characteristics (features), therefore the accuracy of the predictions are discussed and interpreted in relation to these features.

3.1 SINGLE-DEGREE-OF-FREEDOM (SDOF) SYSTEMS

Single-Degree-of-Freedom (SDOF) systems form the foundation of structural dynamics, representing the most basic concept of dynamic response analysis. A linear elastic SDOF system consists of a mass, spring, and damper, and its dynamic behavior is governed by the equation of motion:

$$m\ddot{u}(t) + c\dot{u}(t) + ku(t) = f(t), \tag{3.1}$$

where m is the mass of the system, c is the damping coefficient, k is the stiffness of the system, $u(t)$ is the displacement response, $\dot{u}(t)$ is the velocity response, $\ddot{u}(t)$ is the acceleration response, and $f(t)$ is the external force. In an earthquake excitation, $f(t)$ is equal to $-m\ddot{u}_g(t)$, where $\ddot{u}_g(t)$ is the ground acceleration.

For an elastic SDOF system, the response depends on three key features: (1) the natural period, (2) the damping ratio, and (3) the ground motion. These features characterize the system's dynamic response under seismic loading.

3.1.1 Verification of TCN for SDOF Systems

To verify the Temporal Convolutional Network (TCN) and its implementation for structural response prediction, the first step was to apply TCN to the numerical model of an SDOF system (Figure 3.1) with a natural period of 0.41 seconds and a damping ratio of 2.35%. This configuration matches the dynamic characteristics of San Bernardino 6-story hotel in the NS direction, which is discussed in later sections. A dataset consisting of 10 motions for training[1] and 7 motions

[1] The validation of the training set is a fundamental step in machine learning applications. The training sets used in this study are validated using the discussed metrics, including correlation coefficient, probability distribution of normalized prediction errors and others, refer to Table 3.2 for validation of the used training set for E-W direction response of the San Bernardino 6-story building.

for testing was used, with both recorded ground and total response accelerations (total response acceleration is the sum of ground acceleration and relative response acceleration) of the same building.

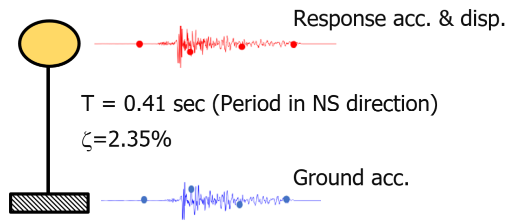

Figure 3.1: Numerical model of an SDOF system.

The TCN predictions showed high accuracy, with a correlation coefficient of 99.99% for the tested motions. The predicted acceleration and displacement time histories matched the computed results with very high accuracy. The predicted and computed (referred to as real) acceleration results are shown in (Figure 3.2) for one of the test motions, the Fontana Earthquake of 25 July 2015. The accuracy of the results are clearly visible in the frequency contents as well.

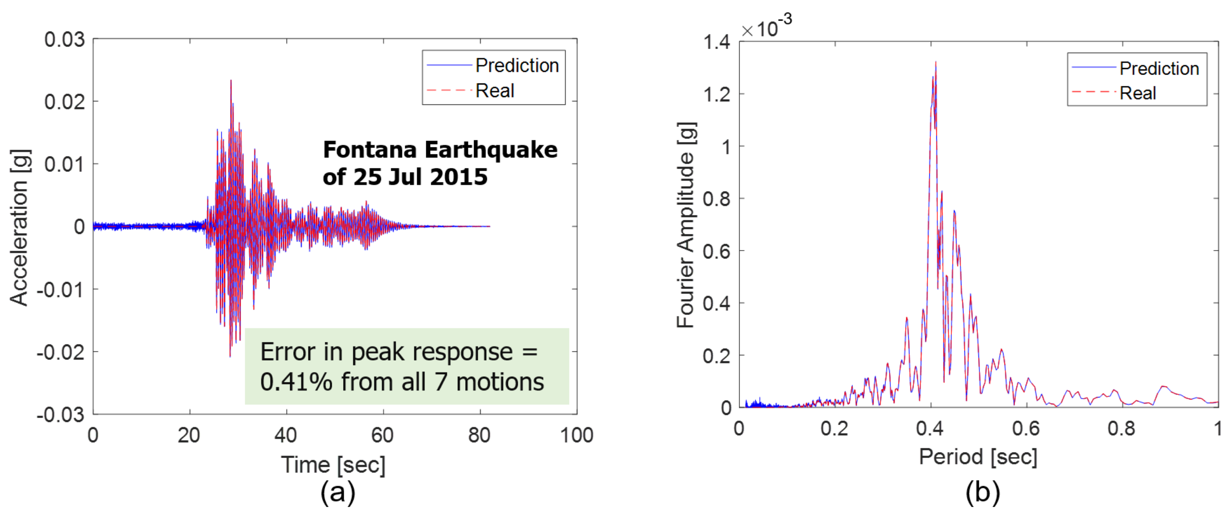

Figure 3.2: Comparison of (a) predicted and recorded acceleration time history and (b) the corresponding frequency contents of the linear elastic SDOF system in Fontana Earthquake of 25 July 2015.

The response of an elastic SDOF system subjected to ground motions is determined solely by its natural period, damping ratio, and the applied ground motion (Table 1.1). The high accuracy of the TCN predictions indicates that the model effectively learned these features. Moreover, these results demonstrate that the training dataset contained sufficient diversity in ground motion characteristics, enabling the TCN to generalize its predictions across various excitations.

The results underline the ability of the TCN model to serve as a reliable and computationally efficient alternative to conventional numerical simulations for predicting linear elastic responses. This basic application developed confidence about the application of TCN on instrumented buildings, experimentally tested structures, and numerical models with more complicated behavior, discussed in the later sections.

3.2 LOW-RISE AND MID-RISE BUILDINGS

Low-rise and mid-rise buildings constitute a significant portion of the built environment and typically exhibit dynamic responses dominated by their fundamental modes of vibration. These structures are well-suited for response prediction using TCN, as their dynamic behavior can be efficiently captured with minimal computational complexity. This section discusses the application of the TCN model to predict linear elastic responses in these building types.

3.2.1 San Bernardino 6-Story RC Hotel Building

Predictions are performed for the linear elastic response of two instrumented CSMIP buildings. The first of these buildings is the 6-story RC Shear Wall (RCSW) hotel building in San Bernardino, California, designed in 1970 (Figure 3.3). This building is instrumented with 9 accelerometers, three on each of the 1st, 3rd, and 6th (roof) floors, and has recorded multiple seismic events from 1987 to 2018. The EW and NS direction responses of this building are studied respectively in this section for the linear response and in a later section for the inelastic response. In the EW direction, Channel 1 on the 1st floor is used as input, and Channels 4 and 7, on the 3rd floor and roof, respectively, are used as outputs. It is noted that the 1st floor boundary conditions are fixed. Therefore, Channel 1 directly represents the ground motion input to the structure. There are a total of 26 events recorded by this station, and 11 and 7 of these records (Table 3.1) are respectively used for training and testing. As shown in Figure 3.5, the motions used in the training set cover the entire range of shaking levels recorded on this building. It is possible to use another Intensity Measure (IM) to define the horizontal axis of this figure. However, the Peak Ground Acceleration (PGA) is used for simplicity as the objective is not to use the IM for quantitative damage detection, but it is rather used to graphically characterize the training and testing set motions as a function of the experienced shaking levels. Eleven motions were sufficient for predicting accurate results for the linear elastic response in the EW direction, and a larger number of motions were utilized for capturing the nonlinear response in the NS direction.

It is noted that unprocessed accelerations are used for all studied instrumented buildings. This is because the processed output is not necessarily the direct result of the processed ground motion input. Therefore, the relationship between the input and output deviates slightly from the true behavior when processed data is used for input and output. This explanation was also supported by the slightly higher accuracy of predictions with unprocessed accelerations as compared to processed accelerations (91% versus 88% in Table 3.2). It is noted that the training accuracy of 0.97 for both the unprocessed and processed data in this table shows that there are no outliers in the set. This high accuracy indicated by the correlation coefficient is also supported by the narrow probability distribution of the normalized error (Equation 2.10) with the mean close to zero (Figure 3.4).

Table 3.1: San Bernardino 6-story hotel training and testing records.

#	Earthquake Name	PGA NS (g)	PFA NS (g)	PGA EW (g)	PFA EW (g)
1	Borrego Springs Area Earthquake of 07 Jul 2010	0.053	0.200	0.024	0.045
2	Devore Earthquake of 29 Dec 2015	0.049	0.106	0.054	0.121
3	Fontana Earthquake of 15 Jan 2014	0.040	0.089	0.034	0.044
4	Inglewood Area Earthquake of 17 May 2009	0.008	0.027	0.008	0.016
5	Ocotillo Area Earthquake of 14 Jun 2010	0.006	0.022	0.006	0.014
6	San Bernardino Earthquake of 08 Jan 2009	0.058	0.168	0.094	0.219
7	Beaumont Earthquake of 14 Sep 2011	0.020	0.041	0.027	0.064
8	La Habra Earthquake of 28 Mar 2014	0.021	0.033	0.024	0.077
9	Loma Linda Earthquake of 13 Mar 2017	0.022	0.050	0.025	0.038
10	Ontario Earthquake of 20 Dec 2011	0.004	0.009	0.004	0.014
11	Yorba Linda Earthquake of 07 Aug 2012	0.009	0.016	0.003	0.010
12	Beaumont Area Earthquake of 16 Jan 2010	0.006	0.013	0.005	0.013
13	Big Bear Lake Earthquake of 05 Jul 2014	0.010	0.030	0.011	0.029
14	Fontana Earthquake of 25 Jul 2015	0.011	0.025	0.010	0.021
15	Loma Linda Earthquake of 08 Oct 2016	0.010	0.017	0.008	0.012
16	Devore Earthquake of 28 Apr 2012	0.017	0.043	0.010	0.029
17	Loma Linda Earthquake of 04 Mar 2013	0.007	0.017	0.012	0.032
18	Chino Hills Earthquake of 29 Jul 2008	0.050	0.113	0.036	0.117

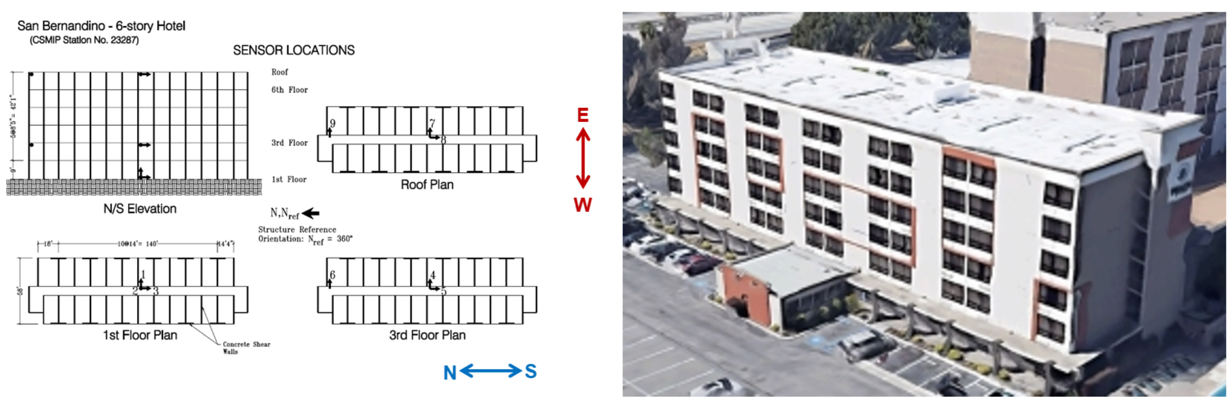

(a) (b)

Figure 3.3: (a) Sensor locations and (b) photograph of the 6-story building in San Bernardino.

The predicted acceleration time histories at the 3rd and 6th (roof) floors are compared with the recorded time histories for one of the test motions (Chino Hills Earthquake of 29 July 2008) in Figure 3.6. This is presented along with the comparison of the frequency contents, showing a close match at both floors in the time and frequency domains.

From a structural dynamics perspective, the linear elastic response of a Multi-Degree of Freedom (MDOF) system depends on the natural periods, damping ratios, and mode shapes. The response of low and mid-rise buildings is generally governed by the first mode, which is also the case for San Bernardino 6-story hotel building. Therefore, similar to the previously discussed SDOF system, the response features are the period and damping ratio of the first mode as well as the ground motion (Table 1.1). The response also depends on the mode shape. However, the first

Table 3.2: **Accuracy of San Bernardino 6-story building acceleration predictions in E-W direction.**

Data	Correlation Coefficient	
	Training Set	Testing Set
Unprocessed	0.97	0.91
Processed	0.97	0.88

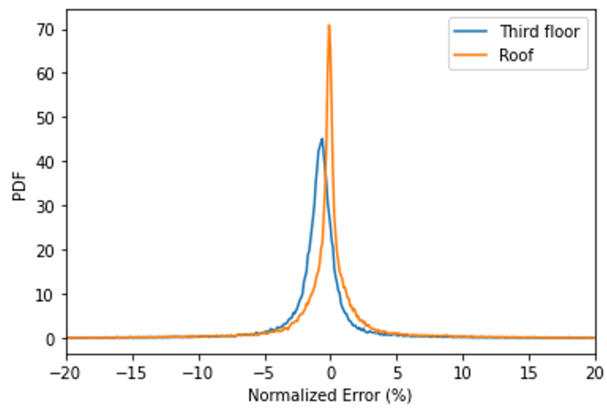

Figure 3.4: Narrow probability distributions of the normalized prediction errors in the EW direction at the 3rd and 6th (roof) floors of the San Bernardino 6-story building.

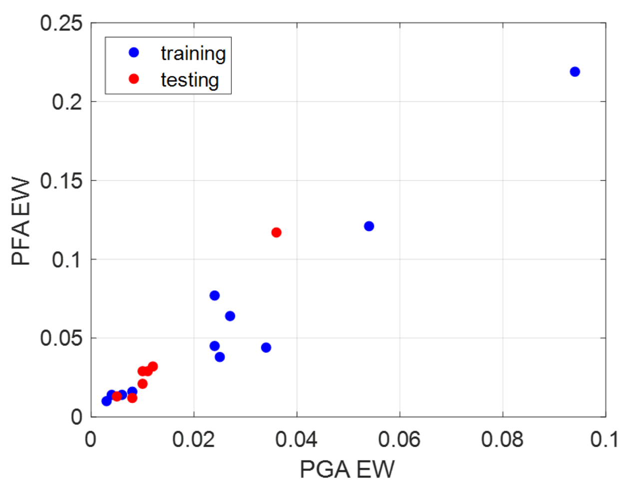

Figure 3.5: The training and testing sets used for San Bernardino 6-story building EW direction.

mode shape amplitude and modal participation factor can be considered as a constant scale factor for all motions. Therefore, the mode shape is not listed as a feature in Table 1.1 for this system.

Although all motions are in the linear elastic range as observed by the natural periods (identified as the period that corresponds to the peak value of the Fourier Amplitude spectra), damping

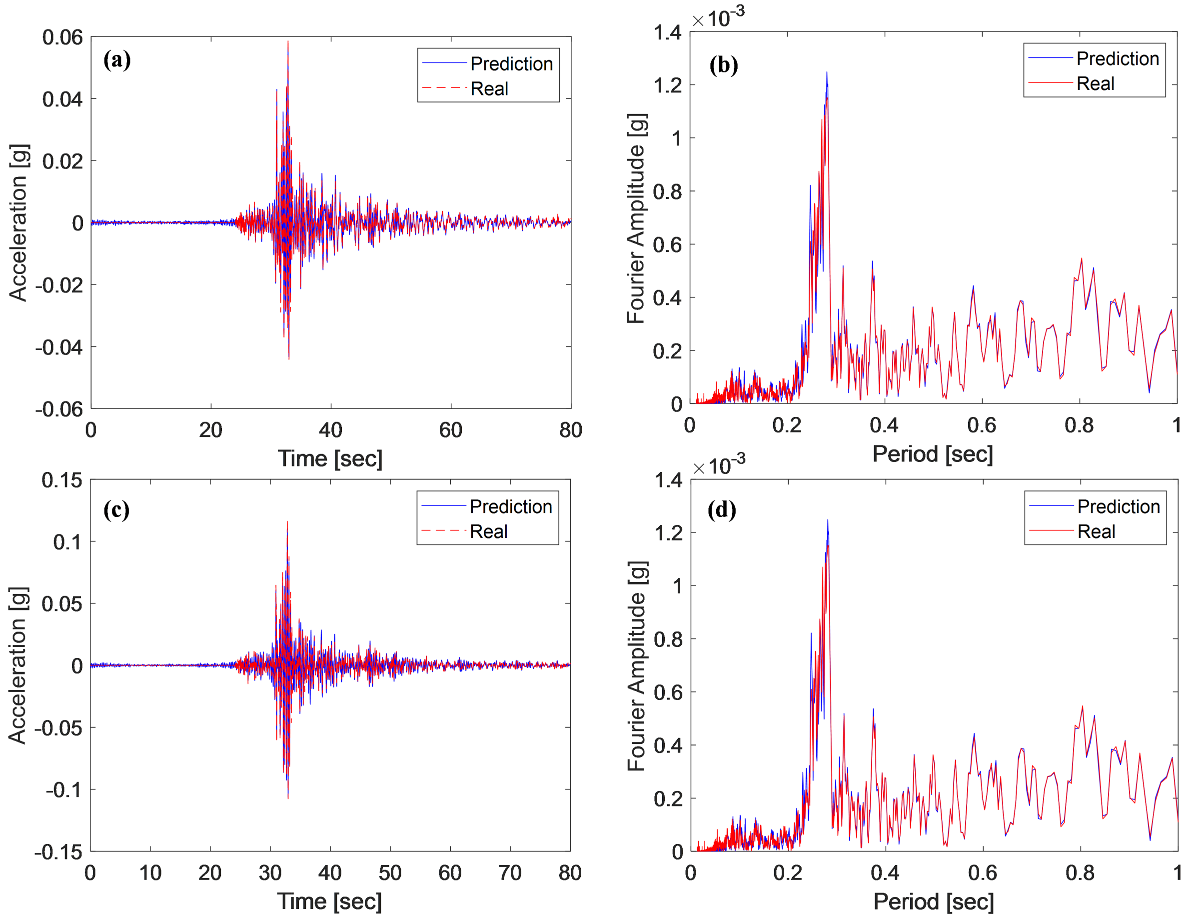

Figure 3.6: Comparison of predicted and recorded acceleration time history and the corresponding frequency contents in the EW direction of San Bernardino 6-story building at (a, b) 3rd floor, (c, d) 6th floor (Chino Hills Earthquake of 29 July 2008).

ratios (identified using the Half-power bandwidth method [5]) vary because of the contribution and complexity of different mechanisms to damping at different intensities (Figure 3.7). The phenomenon of varying damping levels in the linear elastic response is well-known [5, 7]. Even for the same motion in forced vibrations or ambient conditions, the damping ratio varies from segment to segment of the motion [3].

For proper training, the number of motions in the training set should be sufficient and the motions should include a range of intensities to capture different levels of damping ratios. Therefore, a few motions are not sufficient for learning the damping ratio feature as opposed to the case for the period feature, and more motions are needed in the training set to accurately predict the damping. The results of this case study indicated that 10 ground motions were sufficient to learn the period and damping features for consequent accurate predictions.

The success of these predictions highlights the effectiveness of the TCN model in learning key structural features, such as the first mode period and damping ratio, which govern the linear elastic response of low- and mid-rise buildings. This capability underscores the potential of the TCN as a computationally efficient alternative to traditional dynamic analysis methods.

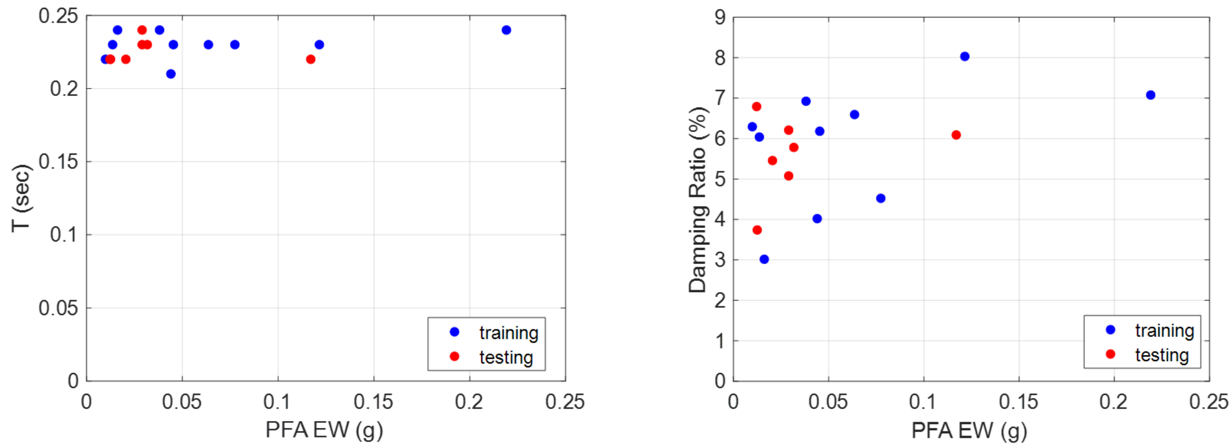

(a) Fundamental mode periods

(b) Damping ratios

Figure 3.7: Identified features (natural periods and damping ratios) for San Bernardino 6-story building.

Performance-based Earthquake Engineering (PBEE) and Damage Assessment

The TCN predictions can be interpreted from the following three perspectives related to their use in PBEE and damage assessment.

1. Epistemic uncertainty is due to errors in mathematical modeling, where the errors due to the TCN model is an example. Due to the presence of epistemic and aleatory uncertainties, the results of a single ground motion are not used in design and assessment of buildings. For example, [1] requires 11 motions for nonlinear dynamic analysis and a varying number of motions (e.g., 20) is essential for probabilistic PBEE [9]. Accordingly, in addition to the individual motion results, comparison of the probability distributions of the true and predicted responses are helpful for evaluating the accuracy of the predictions. The Peak Floor Acceleration (PFA) at the 3rd and 6th floors are assumed to follow a lognormal probability distribution[2] , which are computed using the peak values of all test motions. The resulting probability distributions of true and predicted PFA are plotted in Figure 3.8. It is observed that the resulting probability distributions are close to each other at both floors, illustrating the accuracy of the predictions from this perspective.

2. One of the ways to quantify damage is the use of Engineering Demand Parameter (EDP) based fragility functions, which commonly provide the relationship between peak response

[2] The lognormal probability distribution is developed as a smooth function using its parameters, median and the coefficient of variation. Both parameters for the predicted and real cases are obtained from the peak values in the test motions.

and the probability of damage. The accuracy of TCN predictions can be evaluated using fragility functions and the corresponding damage estimations. As an example, the fragility function of a cooling tower (representing damage to the cooling tower and attached piping), assumed to be located at the roof of San Bernardino 6-story hotel building, is shown in Figure 3.9. This fragility function is defined by a mean of 0.5g and a dispersion of 0.4. The Probability Of Exceedance (POE) of this damage state, using the predicted and true 6th floor PFA for the Chino Hills Earthquake of 07 Aug. 2012, are 5.9% and 6.8%, respectively. In addition to the damage prediction for this single event, the POE in the fragility function, $POE(DM|PFA)$, Figure 3.9, can be integrated with the probability of true and predicted PFA, $p(PFA)$, Figure 3.8b, using the total probability theorem, resulting in the POE of the damage state considering all the test motions, $POE(DM)$, Equation 3.2. It is noted that the probability of the damage state is equal to POE because only one damage state is used herein. Therefore, the resulting probability of damage to a cooling tower located at the roof of the 6-story San Bernardino hotel building, considering all 7 test motions, is 0.33% and 0.30%, respectively, when the true and predicted peaks are used.

3. The above two points discuss the results from a probabilistic PBEE perspective based on peak predictions. However using only the peak response in performance and damage assessment has limitations and the entire response history is important to characterize the full structural behavior. In this context, the Cumulative Absolute Velocity (CAV, Equation 3.3) is a parameter that is closely related to damage and is a suitable metric to evaluate the damage estimation potential of the TCN predictions. Figure 3.10 shows the CAV of the predicted and true accelerations for one of the test motions (Chino Hills Earthquake of 07 Aug. 2012). It is observed from this figure that the CAV time histories of the predicted and true floor accelerations are very close to each other, showing that the predicted response can be used reliably to characterize damage.

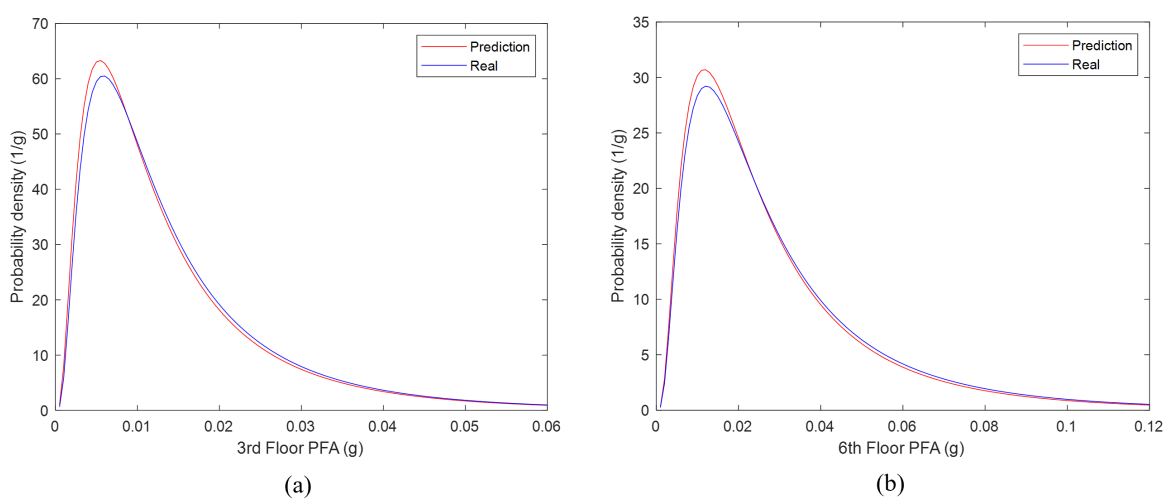

Figure 3.8: Identified features (natural periods and damping ratios) for San Bernardino 6-story building.

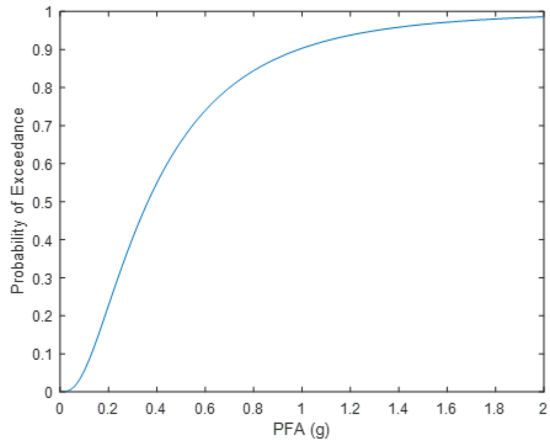

Figure 3.9: Fragility function for a cooling tower assumed to be located at the 6th floor (roof) of San Bernardino 6-story building.

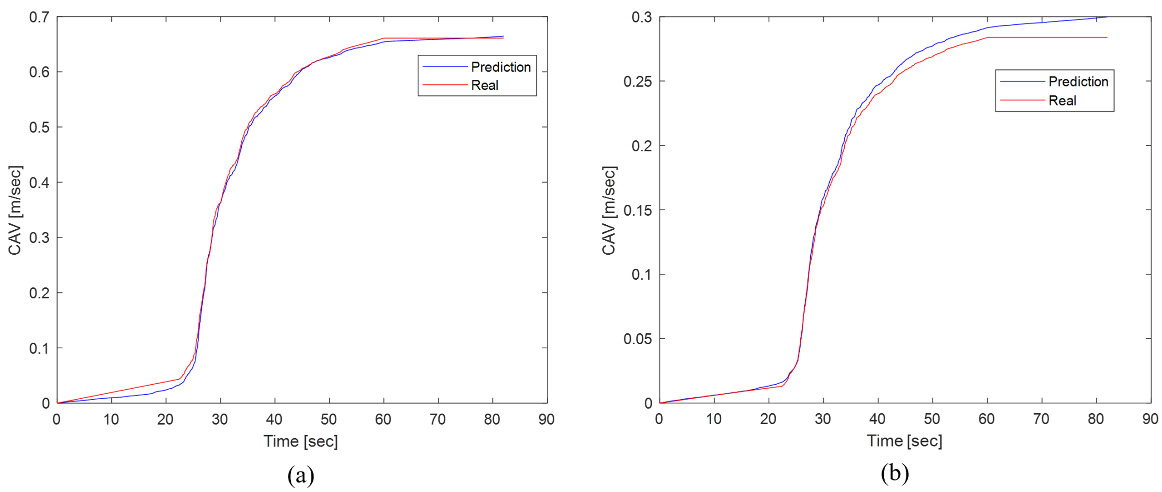

Figure 3.10: CAV of the true and predicted PFA at the (a) 3rd and (b) 6th floors of San Bernardino 6-story building (Chino Hills Earthquake of 07 Aug. 2012).

$$POE(DM) = \sum_{PFA} POE(DM|PFA)p(PFA). \tag{3.2}$$

$$CAV(T) = \int_{t=0}^{T} |\ddot{u}(t)| \, dt, \tag{3.3}$$

where T is the current time at which CAV is computed and $\ddot{u}(t)$ is the response acceleration at a given time t.

Table 3.3: Hemet 4-story building training and testing earthquake records.

#	Earthquake Name	PGA NS (g)	PFA NS (g)	PGA EW (g)	PFA EW (g)
1	Aguanga Earthquake of 14 Aug 2018	0.012	0.031	0.018	0.057
2	Aguanga Earthquake of 19 May 2018	0.007	0.012	0.009	0.024
3	Anza Earthquake of 11 mar 2013	0.011	0.021	0.009	0.013
4	Borrego Springs Earthquake of 10 Jun 2016	0.031	0.071	0.028	0.033
5	Calexico Earthquake of 04 Apr 2010	0.027	0.066	0.037	0.043
6	Valle Vista Earthquake of 10 Feb 2019	0.038	0.049	0.016	0.019
7	Aguanga Earthquake of 20 Dec 2018	0.007	0.018	0.012	0.042
8	Anza Earthquake of 03 Apr 2020	0.017	0.027	0.018	0.042
9	Palomar Observatory Earthquake of 31 Mar 2023	0.009	0.024	0.007	0.010
10	Idyllwild Earthquake of 28 oct 2012	0.045	0.040	0.020	0.025
11	Banning Earthquake of 06 Jan 2016	0.017	0.029	0.015	0.034
12	Cabazon Earthquake of 08 May 2018	0.023	0.058	0.010	0.031
13	San Jacinto Earthquake of 17 Oct 2018	0.017	0.028	0.014	0.023

3.2.2 Hemet 4-Story RC Hospital Building

To demonstrate that accurate predictions are obtained for similar buildings with similar number of records in the training set, a 4-story hospital building with RCSW structural system (similar to San Bernadino Hotel) is tested using the TCN model. This building was designed and constructed in 1965 and instrumented with 10 accelerometers on three levels in 1976 (Figure 3.11). Channel 1 at the basement and Channels 9 (2nd floor) & 6 (4th floor, i.e., roof) are respectively used as input and output in the EW direction. In the NS direction, Channel 3 at the basement and Channels 8 (2nd floor) & 5 (4th floor, i.e., roof) are respectively used as input and output. All these sensors are at the floor centers. From the recorded 13 events, refer to Figure 3.12, 10 are used for training (same number as San Bernardino 6-story building linear elastic response in the EW direction) and 3 are used for testing (Table 3.3). As observed in Figure 3.12, the motions used in the training set cover the entire range of shaking levels recorded on this building and the 3 tested motions are those that lie at the middle of this range.

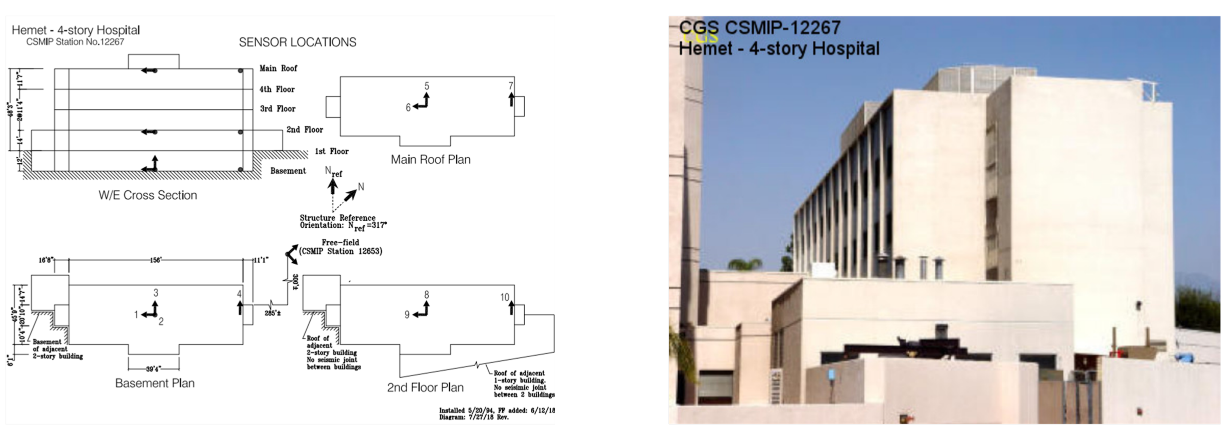

(a) (b)

Figure 3.11: (a) Sensor locations and (b) photograph of the 4-story building in Hemet.

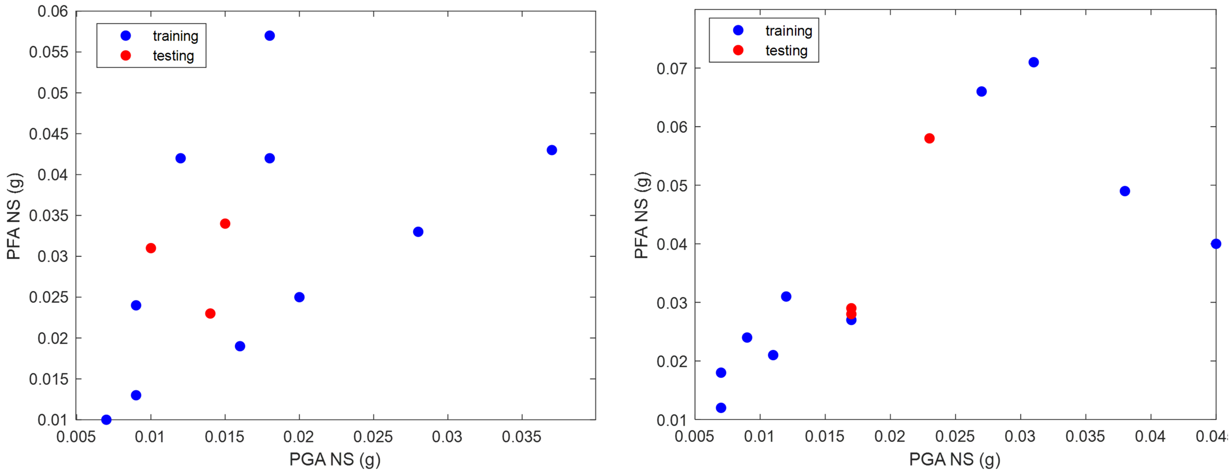

(a) (b)

Figure 3.12: The training and testing sets used for Hemet 4-story building (a) EW, (b) NS directions.

Table 3.4: Accuracy of the Hemet 4-story building acceleration predictions.

Data	**Training Set EW**	**Testing Set EW**	**Training Set NS**	**Testing Set NS**
Unprocessed	97.0%	91.0%	97.0%	90.0%
Processed	97.5%	90.0%	97.5%	90.0%

Similar to San Bernardino building, high correlation coefficients (Table 3.4) and the narrow probability distribution of the normalized error (Figure 3.13)(are obtained for the training and testing sets and unprocessed data provided slightly more accurate predictions. Sample predictions are shown for one of the motions in Figure 3.14, showing the accuracy of the predictions in the NS and EW directions. Similar to San Bernardino building, the TCN model was successful in learning the entire time history of the response of the building, including its natural period and the varying damping ratios, using 10 motions in the training set.

3.3 TALL BUILDINGS WITH HIGHER MODES

Different from low-rise and mid-rise buildings, a tall building seismic response includes higher mode effects. The response of tall buildings involves multiple natural periods, mode shapes, and damping ratios. TCN provides a suitable framework for modeling such systems due to their ability to capture intricate temporal dependencies across multiple modes.

From a structural dynamics perspective, the features that should be accurately characterized for a tall building are the periods and the damping ratios of several modes contributing to the response (Table 1.1). The response also depends on the mode shapes, however, as discussed earlier, the mode shape and the modal participation factor can be considered as a constant scale factor in the linear elastic dynamic response of each mode for each motion and accordingly is not

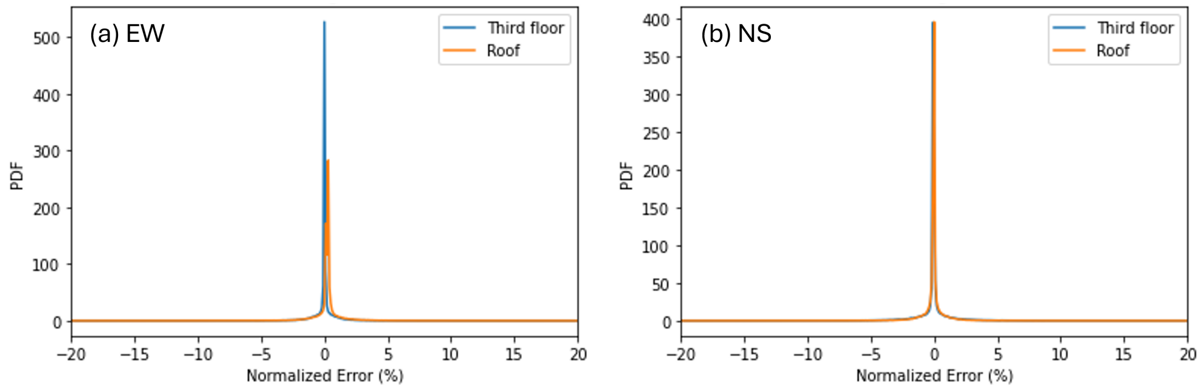

Figure 3.13: Narrow probability distributions of the normalized prediction errors at the 3rd and roof floors of the Helmet 4-story building: (a) EW, and (b) NS directions.

considered as an explicit factor that the response depends on. Considering the increased number of features, the presence of multiple modes in the response may introduce additional challenges to the process of learning, impacting the accuracy of the predictions. Therefore, a 54-story instrumented building is selected to explore the TCN predictions for a case where higher modes are clearly present in the response. This 54-story building is a Steel Moment Resisting Frame (SMRF) building with composite slabs of 2.5 inches thick concrete over 3 inches steel deck located in Los Angeles (LA), Figure 3.15. From this figure, it is observed that the building is instrumented with 20 accelerometers at the basement (4 levels below ground), ground level, and the 20th, 36th, 46th and the penthouse floors. There are Vierendeel trusses and 48-inch-deep transfer girders at the 36th and 46th floors where vertical setbacks occur. Because there is a sudden change of stiffness at these locations, increased accelerations are expected, and sensors are placed at these floors for monitoring this expected increase of accelerations.

In this case study building, which has 11 recorded motions, 10 motions are used for training and the remaining one motion is used for testing (Figure 3.16). The testing motion in the EW direction is particularly interesting as the Peak Floor Acceleration (PFA) is smaller than the corresponding PGA. This is attributed to: (a) the shape of the response spectrum for this motion, where the response acceleration at the first mode period of the building is smaller than the PGA, and (b) multiple modes counteracting and reducing the accelerations. The successful predictions in the EW and NS[3] directions at the 46th floor for the considered test motion are shown in Figure 3.17. This figure demonstrates that the trained TCN model is successful in learning more complex responses obtained as a superposition of multiple modes and the 10-motion training set results in

[3] As observed in the floor plans and building photograph, Figure 3.15, this building is fairly symmetric about its orthogonal axes. Coupling between these two orthogonal directions could be due to mass center eccentricity, which is also expected to be minimal given the floor plans without area expansions. Therefore, the coupling between the responses in the two horizontal directions is expected to be minimal and the EW and NS responses are governed by the respective motions in these directions. However, there are instrumented buildings in the CSMIP database, such as buildings with L-shaped plans, where the response in one horizontal direction would depend not only on the ground motion component in that direction, but also on the one in the orthogonal direction, through coupling from the stiffness matrix. Such response requires adapting the TCN for multiple input vectors. This is also true for multi-support excitation as in long-span bridges. This is a planned topic for future studies.

accurate responses as in the cases of San Bernardino and Hemet buildings.

The TCN predictions showed high accuracy, as demonstrated by the time-history and frequency-domain comparisons for the test motion. The model successfully captured the complex response resulting from (i) the superposition of multiple modes, (ii) sudden stiffness change, validating its capability to handle higher mode effects.

The response of a tall building is influenced by contributions from multiple modes, however the contribution of these modes to the response varies from motion to motion. To enable the TCN model to learn about the contributions of higher modes effectively, it is needed to include motions in the training set that sufficiently excite these modes. Figure 3.18 shows the normalized amplification function in the EW and NS directions for the training and testing motions. Amplification function is computed as the Fourier amplitude of the 46th story response acceleration divided by the Fourier amplitude of the input ground acceleration. The resulting amplification function is normalized by the maximum value of this amplification function. It is observed from Figure 3.18 that the second and third modes of vibration are excited to varying levels in the training motions, with amplification function values at these modes approaching and exceeding that of the first mode in several motions. The presence of these higher modes in that training set enables the TCN model to learn the contributions of these modes, resulting in accurate predictions. The presence of the 2nd mode contribution in the NS direction of the test motion is clearly visible, and the accurate predictions in this direction highlight that the TCN model with the motions in the training set was successful in capturing the contribution of this mode.

The accurate predictions for tall buildings highlight the potential of TCN to model complex dynamic responses involving higher modes. Unlike conventional dynamic analysis methods, which often require a detailed structural analysis model, TCN provides a more efficient alternative while maintaining high accuracy. This efficiency makes TCN particularly valuable for applications such as performance-based earthquake engineering and structural health monitoring of tall buildings.

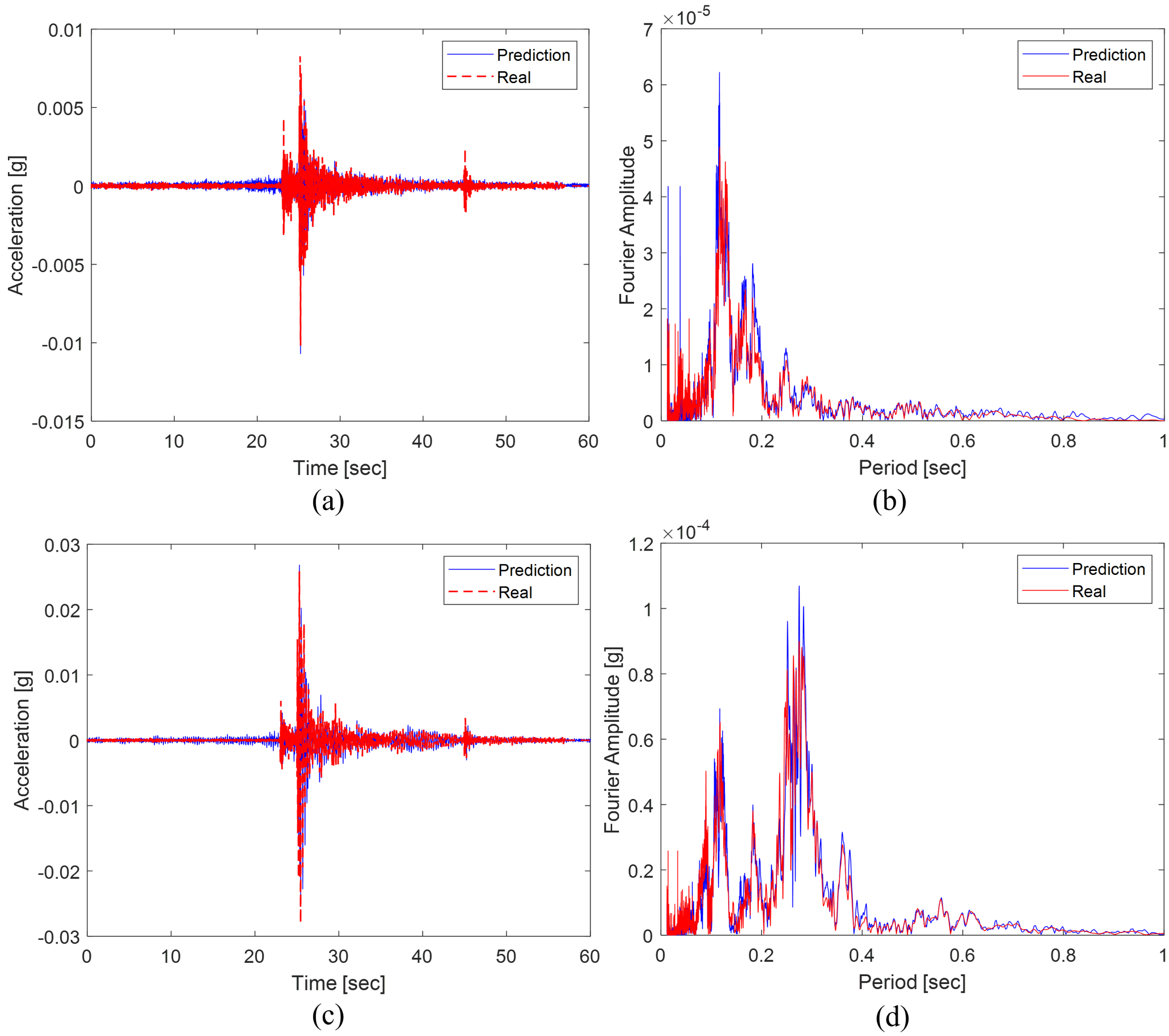

Figure 3.14: Comparison of predicted and recorded acceleration time history and the corresponding frequency contents in the (a, b) EW and (c, d) NS directions of Hemet 4-story building (Banning Earthquake of 06 Jan 2016).

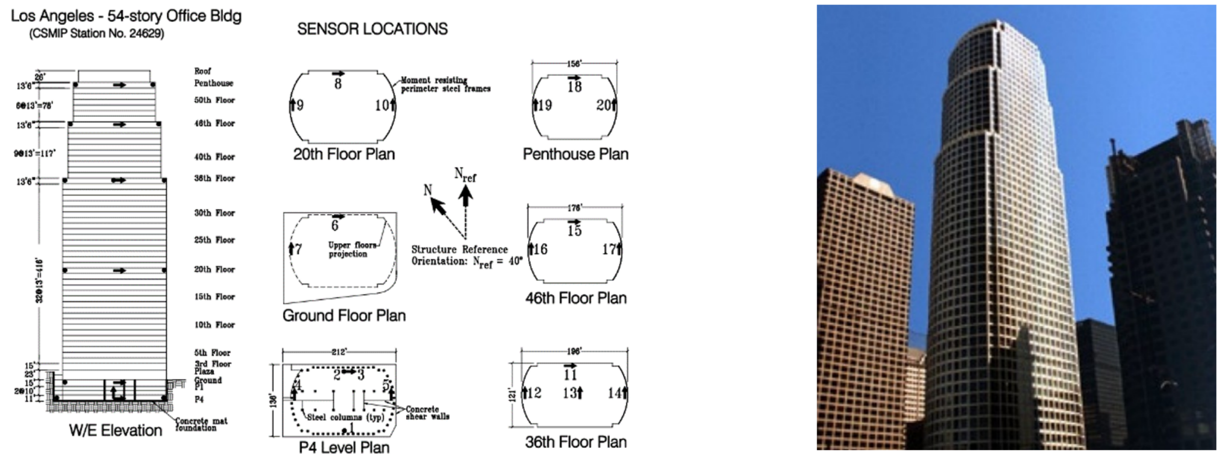

(a) (b)

Figure 3.15: (a) Sensor locations and (b) photograph of the 54-story building in Los Angeles.

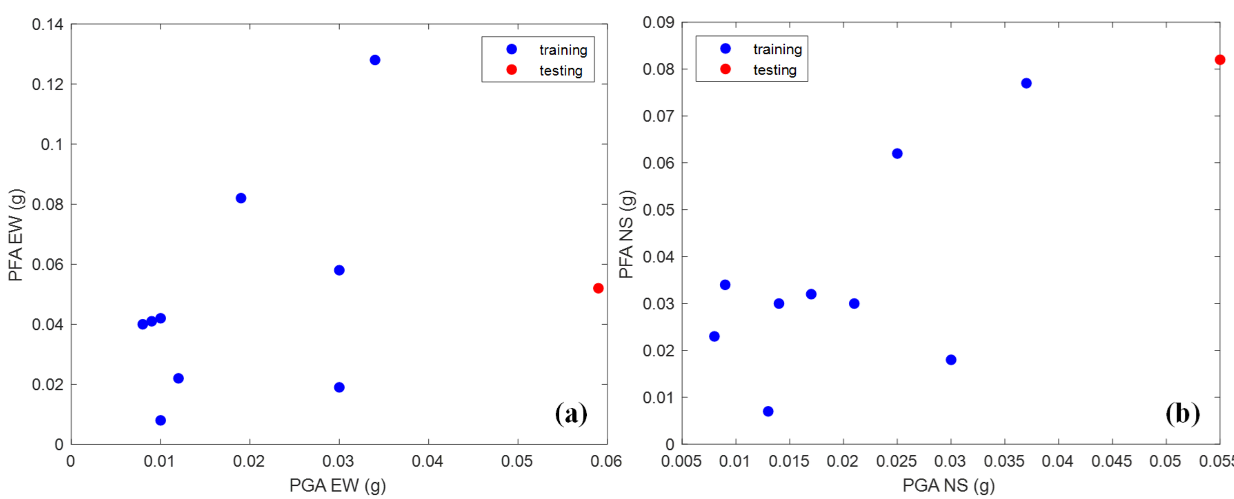

Figure 3.16: Training and testing sets used for LA 54 story building (a) EW, and (b) NS directions.

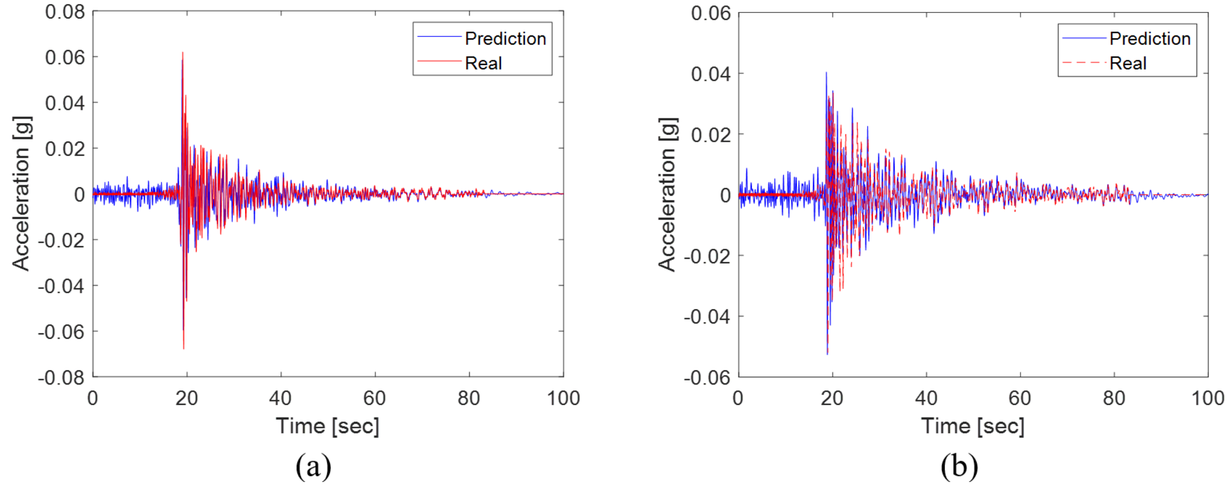

Figure 3.17: The 46th story acceleration predictions for the 56-story building in LA: (a) EW, and (b) NS directions (Chino Hills Earthquake of 29 July 2008).

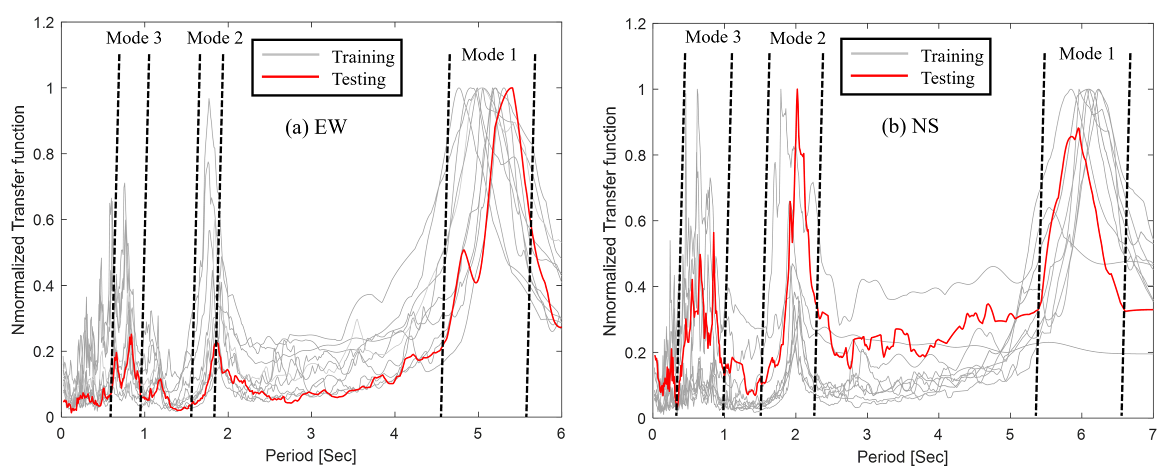

Figure 3.18: Normalized amplification functions for the 56-story building in LA: (a) EW, and (b) NS directions.

4 Inelastic Response Prediction

Instrumented structures provide valuable data for understanding the inelastic behavior of buildings under seismic loading. The nonlinear response involves phenomena such as cracking, yielding, buckling, fracture, and period elongation, the modeling of which introduces challenges to the numerical integration methods used to solve the equations of motions in nonlinear dynamic analysis. This section discusses the inelastic response predictions conducted using TCN for three case studies: a mid-rise building subjected to real earthquakes, a low-rise structure tested in a laboratory setting, and an inelastic SDOF numerical model.

4.1 SAN BERNARDINO 6-STORY RC HOTEL BUILDING (NS DIRECTION)

The identified periods of this building in the EW direction are almost constant in the tight range of 0.21 to 0.24 sec, independent of the level of shaking, which is indicative of linear elastic response (Figure 4.1). On the other hand, the periods in the NS direction clearly increase with the level of shaking, indicating inelastic response (Figure 4.1). Although it is not entirely clear why this period elongation occurred since the set of training ground motions include low-level motions, possible reasons can be minor cracking, foundation rocking, disengagement of partition walls providing stiffness, or loss of contributions from other nonstructural components.

Although the inelastic response of this case study is not extensive, it presents a more challenging case for prediction compared to the linear elastic response. To predict the inelastic response in the NS direction, the same 10 motions used in the EW direction were not sufficient. As observed in Table 1.1, the features that need to be characterized for predicting the linear elastic and inelastic responses of a low- or mid-rise building is the first mode period and the first mode period elongation, respectively. The accurate characterization of period elongation requires not only a larger number of motions, but also the use of motions that span the entire range of period elongation. As mentioned earlier, the total number of events recorded for this building is 32 (Table 4.1.) Out of these 32 motions, 29 covering the entire range of shaking levels were used for training as shown in Figure 4.2 and three events in the middle of the intensity range of these motions are used for testing. The results show the increased accuracy of the predictions as demonstrated in Figures 4.3, 4.4, and 4.5 for the motions in the testing set. Particularly, the time history, the peaks, and the frequency contents are well matched, indicating that increasing the number of motions in the training set from 11 to 23 led to successful characterization of the increase of the period elongation with increased shaking intensity.

Table 4.1: Training and testing earthquake records with PGA and PFA values.

#	Earthquake Name	PGA (g)	PFA (g)
1	Big Bear Lake Earthquake of 05 Jul 2014	0.010	0.030
2	Inglewood Area Earthquake of 17 May 2009	0.008	0.027
3	Fontana Earthquake of 25 Jul 2015	0.011	0.025
4	La Verne Earthquake of 28 Aug 2018	0.008	0.025
5	Anza Earthquake of 03 Apr 2020	0.007	0.023
6	Ocotillo Area Earthquake of 14 Jun 2010	0.006	0.022
7	Little Lake Earthquake of 05 Jul 2019	0.004	0.021
8	Loma Linda Earthquake of 30 Jan 2019	0.008	0.019
9	Trabuco Canyon Earthquake of 25 Jan 2018	0.010	0.019
10	Searles Valley Earthquake of 03 Jun 2020	0.004	0.018
11	Loma Linda Earthquake of 04 Mar 2013	0.007	0.017
12	Loma Linda Earthquake of 08 Oct 2016	0.010	0.017
13	Yorba Linda Earthquake of 07 Aug 2012	0.009	0.016
14	Loma Linda Earthquake of 23 Jun 2008	0.013	0.016
15	Beaumont Area Earthquake of 16 Jan 2010	0.013	0.013
16	Banning Area Earthquake of 11 Jan 2010	0.005	0.011
17	Ontario Earthquake of 20 Dec 2011	0.004	0.009
18	Borrego Springs Area Earthquake of 07 Jul 2010	0.053	0.200
19	Borrego Springs Earthquake of 10 Jun 2016	0.042	0.188
20	San Bernardino Earthquake of 08 Jan 2009	0.058	0.168
21	Ridgecrest Earthquake of 05 Jul 2019	0.029	0.120
22	Chino Hills Earthquake of 29 Jul 2008	0.050	0.113
23	Devore Earthquake of 29 Dec 2015	0.049	0.106
24	Calexico Earthquake of 04 Apr 2010	0.019	0.105
25	Fontana Earthquake of 15 Jan 2014	0.040	0.089
26	Loma Linda Earthquake of 13 Mar 2017	0.022	0.050
27	Devore Earthquake of 28 Apr 2012	0.017	0.043
28	Beaumont Earthquake of 14 Sep 2011	0.020	0.041
29	La Habra Earthquake of 28 Mar 2014	0.024	0.038
30	Cabazon Earthquake of 08 May 2018	0.027	0.048
31	Redlands Area Earthquake of 13 Feb 2010	0.082	0.074
32	Banning Earthquake of 06 Jan 2016	0.021	0.069

These successful predictions highlight an important and unique characteristic of obtaining the response using a deep learning approach. Several reasons cause the observed period elongation with increased intensity of shaking (e.g., concrete cracking, foundation rocking, and disengagement of partition walls, or loss of contributions from other nonstructural components). In common practice, none of these aspects are considered explicitly in the computational models developed for structural dynamic analysis. Even if they are modeled, there are many sources of increased epistemic uncertainties associated with this type of modeling. Therefore, the obtained data-driven TCN results show that the adopted deep learning approach fills this gap and results in accurate structural response prediction that would not be possible using conventional dynamic analysis. This case study also highlights two important aspects worthy of future investigation, namely, the

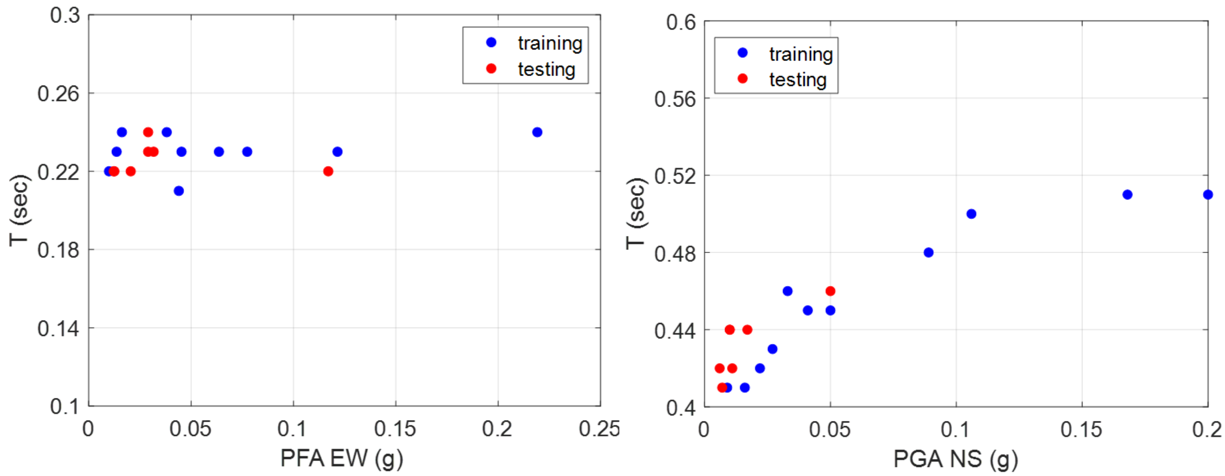

(a) (b)

Figure 4.1: Identified periods of San Bernardino 6-story hotel building in (a) EW, and (b) NS directions in different earthquakes.

effect of increased size of the training dataset (justifying need for more instrumented systems) and a hybrid use of physics-based and data-driven models where the data-driven model improves the predictions in cases where the physics-based modeling capabilities are insufficient.

4.2 LABORATORY TESTING OF A 3-STORY REPEAT FRAME

Some instrumented buildings exist in the Center for Engineering Strong Motion Data (CESMD) database which experienced damage in previous earthquakes, e.g., the 7-story hotel in Van Nuys damaged in the 1994 Northridge earthquake. However, the number of earthquakes with inelastic response in these buildings is limited for meaningful training. Therefore, the results from a shaking table test are used as another system to predict its inelastic response.

The tested structure is a 3-story SMRF and was tested on the 6 Degree-of-Freedom (DOF) PEER (Pacific Earthquake Engineering Research) Center shaking table at UC-Berkeley. The photographs of the tested structure are shown in Figure 4.6. The frame is assembled using steel beam-column elements, cross-joints, and clevises. The beams and columns are 65 in long, 5 in $\times$ 5 in $\times$ 3/8 in Hollow Square Section (HSS) members. There are 1 in thick plates at each end of the members to attach them to the beam-column connections. The cross-joints at the connections are composed of the same HSS profile and plates.

The structure is tested along the Y-direction only by applying ground motions to the table. Along this direction, beams are connected to the cross-joints using clevises and coupons (Figure 4.6c), resulting in semi-rigid connections. The flexural stiffness of these connections is provided by a couple moment developed by the coupons. Following the principles of capacity design, the sizes and number of coupons are selected such that the capacity of this couple moment is smaller than the yield moment of the beam HSS section to protect the beams from yielding. Thus, the damage occurs only at the coupons (Figure 4.6d), which can be easily replaced, and the frame

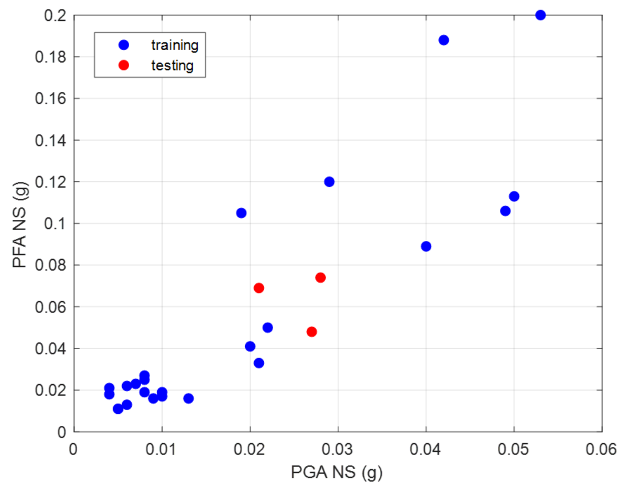

Figure 4.2: Training and testing sets for San Bernardino 6-story building NS direction.

reconstructed conveniently each time after destructive testing (thus, the name **REPEAT** stands for **RE**configurable **P**latform for **EA**rthquake **T**esting). The columns are directly connected to the cross-joints resulting in rigid connections. Following principles of earthquake design, columns are designed to be stronger than beams, preventing the yielding of columns. There are two 3/4 in diameter threaded bars on the outside of each column clevis at the base (Figure 4.6b). Each beam-column joint has four of these threaded bars, two on each side of the clevis (Figure 4.6c).

The test matrix is shown in Table 4.2. Three ground motions are applied incrementally leading to linear elastic and inelastic response of the structure. Two of these motions are the ground motions recorded during the 1989 Loma Prieta earthquake. The third is a simulated ground motion obtained from physics-based simulations of San Francisco Bay Area. In such simulations, a numerical model of the geologic and local soil layers is developed in a large area (e.g., the entire San Francisco Bay Area) and the ground motions at the earth's surface and subsurface are computed at closely spaced grid points. This is obtained from the numerical solution of the viscoelastic wave equation in both space and time initiated by a fault rupture model [15]. These simulated ground motions are validated against recorded ground motions in real earthquakes, and they are part of the PEER Center effort to develop a Simulated Ground Motion Database (SGMD), to be publicly available during Fall of 2025.

Table 4.2: Test matrix used in the shaking table tests.

Run #	Ground Motion	Scale Factor	Run #	Ground Motion	Scale Factor
1	Simulated motion	0.25	10	Simulated motion	1.00
2	Loma Prieta Sunnyvale Station	0.25	11	Loma Prieta Sunnyvale Station	1.00
3	Loma Prieta Palo Alto Station	0.25	12	Loma Prieta Palo Alto Station	1.00
4	Simulated motion	0.50	13	Simulated motion	1.25
5	Loma Prieta Sunnyvale Station	0.50	14	Loma Prieta Sunnyvale Station	1.25
6	Loma Prieta Palo Alto Station	0.50	15	Loma Prieta Palo Alto Station	1.25
7	Simulated motion	0.75	16	Loma Prieta Palo Alto Station	1.50
8	Loma Prieta Sunnyvale Station	0.75	17	Loma Prieta Palo Alto Station	1.75
9	Loma Prieta Palo Alto Station	0.75			

In all tests, the applied ground motions were recorded on the table, along with the response accelerations at the center of each of the three floors. Inelastic response was experienced in runs 10-17 as observed by the period elongation in Figure 4.7, and the buckled coupons in Figure 4.6d. Predictions were conducted using two training sets. First training set included runs 1-13, with a mix of linear elastic and inelastic responses and predicted the inelastic responses in runs 14-17. The predicted acceleration response at the third floor in run 17 is compared with the recorded response in Figure 4.8. The prediction is reasonable in the time domain; however, it fails to capture the period elongation in the frequency domain. Although the training set covers the entire range of response, this is an indication that the number of motions in the training set is not sufficient. Accordingly, the number of motions in the second training set was increased to 16 (runs 1-16), while only run 17 was used for testing. Figure 4.9 shows the improved predictions, where the time history of the predicted acceleration response is close to the true acceleration response and the period elongation is captured. It is also observed that the predicted acceleration response includes the 2nd and 3rd mode natural frequencies in the frequency content, similar to the recorded response.

The fragility functions for the three damage states of a suspended ceiling is shown in Figure 4.10. The considered suspended ceiling is a Suspended Lay-in Acoustic Tile Ceiling, with supports comprising vertical hanging wire, diagonal wires, and compression posts. The damage states are defined as 5% (DS1), 30% (DS2), and 50% (DS3) of ceiling grid and tile damage. The fragility functions for these damage states are cumulative lognormal and are defined as a function of PFA. The median PFA for DS1, DS2, and DS3 are 1.92g, 2.34g, and 2.48g, with a Coefficient of Variation (COV) of 0.3 in all damage states. It is assumed that such suspended ceiling is placed at the 3rd floor of the tested structure and the probabilities of the three damage states are computed using the predicted and recorded accelerations. Probabilities of DS1, DS2,and DS3 are 5%, 3%, and 91% using the predicted PFA of 3.32g, while they are 9%, 4%, and 84% using the recorded PFA of 3.69g. Similar to the good match between computed and measured accelerations, there is a good match between the corresponding probabilities of nonstructural damage.

4.3 SDOF INELASTIC NUMERICAL MODEL

The characteristics of the SDOF system used for prediction of inelastic response is shown in Figure 4.11a. This SDOF system is developed to be representative of low- and mid-rise buildings and has a period of 0.5 s and damping ratio of 5%. Considering a location with design acceleration of 1.0g, Response Modification Factor (R) of 8, and overstrength of 1.6, the yield base shear (F_y) is 20% of the weight W. The force-deformation relationship is bilinear with a strain hardening ratio of 1.0% of initial stiffness. Ninety-three motions with varying intensity levels were selected from the PEER Ground Motion (GM) database, and nonlinear time history analyses were conducted using these 93 motions. From these input – output (i.e., ground motion – computed response acceleration), 83 and 10 time-histories (Tables 4.3 and 4.4) were used for training and testing, respectively. Note that in Tables 4.3 and 4.4, M_w and RSN indicate moment magnitude and Record Sequence Number, respectively. To predict the inelastic response, the training set covers the entire range of linear elastic and inelastic responses, while the testing set includes the analyses with moderate to very high levels of inelastic response, i.e., ductility demands between 6 and 14. (Figure 4.11b).

Table 4.3: Training ground motions for the inelastic SDOF system.

#	RSN	Earthquake			Station	Component	PGA (g)
		Name	Year	M_w			
1	120	Oroville-03	1975	4.7	Up & Down Cafe (OR1)	000	0.11
2	195	Imperial Valley-07	1979	5.0	Calexico Fire Station	225	0.09
3	197	Imperial Valley-07	1979	5.0	El Centro Array #1	140	0.06
4	199	Imperial Valley-07	1979	5.0	El Centro Array #11	140	0.19
5	200	Imperial Valley-07	1979	5.0	El Centro Array #2	140	0.13
6	201	Imperial Valley-07	1979	5.0	El Centro Array #3	140	0.13
7	193	Imperial Valley-07	1979	5.0	Bonds Corner	140	0.10
8	194	Imperial Valley-07	1979	5.0	Brawley Airport	225	0.05
9	195	Imperial Valley-07	1979	5.0	Calexico Fire Station	225	0.09
10	101	Northern Calif-07	1975	5.2	Cape Mendocino	030	0.16
11	103	Northern Calif-07	1975	5.2	Petrolia, General Store	075	0.15
12	42	Lytle Creek	1970	5.3	Cedar Springs Pumphouse	126	0.07
13	45	Lytle Creek	1970	5.3	Devil's Canyon	090	0.17
14	50	Lytle Creek	1970	5.3	Wrightwood - 6074 Park Dr	115	0.17
15	21	Imperial Valley-05	1955	5.4	El Centro Array #9	000	0.04
16	217	Livermore-02	1980	5.4	APEEL 3E Hayward CSUH	146	0.04
17	218	Livermore-02	1980	5.4	Antioch - 510 G St	270	0.08
18	219	Livermore-02	1980	5.4	Del Valle Dam (Toe)	156	0.04
19	223	Livermore-02	1980	5.4	San Ramon - Eastman Kodak	180	0.20
20	27	Hollister-02	1961	5.5	Hollister City Hall	181	0.06
21	125	Friuli, Italy-01	1976	6.5	Tolmezzo	000	0.32
22	161	Imperial Valley-06	1979	6.5	Brawley Airport	225	0.18
23	162	Imperial Valley-06	1979	6.5	Calexico Fire Station	225	0.24
24	165	Imperial Valley-06	1979	6.5	Chihuahua	012	0.27
25	167	Imperial Valley-06	1979	6.5	Compuertas	015	0.15
26	170	Imperial Valley-06	1979	6.5	EC County Center FF	002	0.22
27	173	Imperial Valley-06	1979	6.5	El Centro Array #10	050	0.20
28	174	Imperial Valley-06	1979	6.5	El Centro Array #11	140	0.37
29	178	Imperial Valley-06	1979	6.5	El Centro Array #3	140	0.26
30	184	Imperial Valley-06	1979	6.5	El Centro Differential Array	270	0.44
31	185	Imperial Valley-06	1979	6.5	Holtville Post Office	225	0.24
32	187	Imperial Valley-06	1979	6.5	Parachute Test Site	225	0.17
33	192	Imperial Valley-06	1979	6.5	Westmorland Fire Sta	090	0.08
34	71	San Fernando	1971	6.6	Lake Hughes #12	021	0.32
35	952	Northridge-01	1994	6.7	Beverly Hills - 12520 Mulhol	035	0.54
36	960	Northridge-01	1994	6.7	Canyon Country - W Lost Cany	000	0.40
37	986	Northridge-01	1994	6.7	LA - Brentwood VA Hospital	285	0.18
38	989	Northridge-01	1994	6.7	LA - Chalon Rd	160	0.20
39	996	Northridge-01	1994	6.7	LA - N Faring Rd	090	0.27
40	1006	Northridge-01	1994	6.7	LA - UCLA Grounds	360	0.39
41	1012	Northridge-01	1994	6.7	LA 00	270	0.34
42	1042	Northridge-01	1994	6.7	N Hollywood - Coldwater Can	270	0.27

Table 4.3: Training ground motions for the inelastic SDOF system, continued.

#	RSN	Earthquake			Station	Component	PGA (g)
		Name	Year	M_w			
43	1049	Northridge-01	1994	6.7	Pacific Palisades - Sunset	280	0.34
44	1052	Northridge-01	1994	6.7	Pacoima Kagel Canyon	360	0.37
45	1054	Northridge-01	1994	6.7	Pardee - SCE	–T	0.42
46	1082	Northridge-01	1994	6.7	Sun Valley - Roscoe Blvd	090	0.35
47	1083	Northridge-01	1994	6.7	Sunland - Mt Gleason Ave	260	0.15
48	1089	Northridge-01	1994	6.7	Topanga - Fire Sta	270	0.26
49	1111	Kobe, Japan	1995	6.9	Nishi-Akashi	090	0.47
50	763	Loma Prieta	1989	6.9	Gilroy - Gavilan Coll.	067	0.34
51	764	Loma Prieta	1989	6.9	Gilroy - Historic Bldg.	160	0.28
52	767	Loma Prieta	1989	6.9	Gilroy Array #3	000	0.50
53	768	Loma Prieta	1989	6.9	Gilroy Array #4	000	0.31
54	803	Loma Prieta	1989	6.9	Saratoga - W Valley Coll.	000	0.30
55	809	Loma Prieta	1989	6.9	UCSC	000	0.37
56	810	Loma Prieta	1989	6.9	UCSC Lick Observatory	000	0.46
57	6	Imperial Valley-02	1940	7.0	El Centro Array #9	180	0.23
58	864	Landers	1992	7.3	Joshua Tree	000	0.27
59	1148	Kocaeli, Turkey	1999	7.5	Arcelik	090	0.17
60	1161	Kocaeli, Turkey	1999	7.5	Gebze	270	0.19
61	1193	Chi-Chi, Taiwan	1999	7.6	CHY024	000	0.23
62	1198	Chi-Chi, Taiwan	1999	7.6	CHY029	000	0.27
63	1201	Chi-Chi, Taiwan	1999	7.6	CHY034	270	0.30
64	1202	Chi-Chi, Taiwan	1999	7.6	CHY035	000	0.26
65	1244	Chi-Chi, Taiwan	1999	7.6	CHY101	000	0.38
66	1488	Chi-Chi, Taiwan	1999	7.6	TCU048	000	0.13
67	1490	Chi-Chi, Taiwan	1999	7.6	TCU050	000	0.14
68	1491	Chi-Chi, Taiwan	1999	7.6	TCU051	000	0.19
69	1493	Chi-Chi, Taiwan	1999	7.6	TCU053	000	0.19
70	1494	Chi-Chi, Taiwan	1999	7.6	TCU054	000	0.17
71	1495	Chi-Chi, Taiwan	1999	7.6	TCU055	000	0.22
72	1496	Chi-Chi, Taiwan	1999	7.6	TCU056	000	0.16
73	1497	Chi-Chi, Taiwan	1999	7.6	TCU057	000	0.11
74	1499	Chi-Chi, Taiwan	1999	7.6	TCU060	000	0.15
75	1501	Chi-Chi, Taiwan	1999	7.6	TCU063	000	0.16
76	1515	Chi-Chi, Taiwan	1999	7.6	TCU082	000	0.20
77	1519	Chi-Chi, Taiwan	1999	7.6	TCU087	000	0.12
78	1527	Chi-Chi, Taiwan	1999	7.6	TCU100	000	0.11
79	1530	Chi-Chi, Taiwan	1999	7.6	TCU103	000	0.16
80	1531	Chi-Chi, Taiwan	1999	7.6	TCU104	000	0.10
81	1533	Chi-Chi, Taiwan	1999	7.6	TCU106	000	0.15
82	1535	Chi-Chi, Taiwan	1999	7.6	TCU109	000	0.16
83	1536	Chi-Chi, Taiwan	1999	7.6	TCU110	000	0.18

Table 4.4: Testing ground motions for the inelastic SDOF system.

#	RSN	Earthquake			Station	Component	PGA (g)
		Name	Year	M_w			
84	752	Loma Prieta	1989	6.9	Capitola	000	0.47
85	765	Loma Prieta	1989	6.9	Gilroy Array #1	000	0.43
86	766	Loma Prieta	1989	6.9	Gilroy Array #2	000	0.36
87	801	Loma Prieta	1989	6.9	San Jose - Santa Teresa Hills	225	0.28
88	802	Loma Prieta	1989	6.9	Saratoga - Aloha Ave	000	0.37
89	811	Loma Prieta	1989	6.9	WAHO	000	0.54
90	953	Northridge-01	1994	6.7	Beverly Hills - 14145 Mulhol	009	0.44
91	1101	Kobe, Japan	1995	6.9	Amagasaki	090	0.31
92	1158	Kocaeli, Turkey	1999	7.5	Duzce	270	0.32
93	1182	Chi-Chi, Taiwan	1999	7.6	CHY006	6-W	0.36

The prediction results from ground motion GM93 (Figure 4.12) are shown in Figure 4.12. The force-displacement relationship in Figure 4.12e represents a highly inelastic response. The pattern of the predicted acceleration matches the true response well, both in the linear elastic and inelastic response ranges. The frequency content and the period elongation are well-captured. The main issue is the overestimated accelerations in the inelastic response range, where the computed acceleration response was capped around 0.25g, which is explained using the following equation of motion of an inelastic SDOF system:

$$m\ddot{u} + c\dot{u} + f_r = 0, \tag{4.1}$$

where m is the mass, c is the damping coefficient, and f_r is the restoring force of the SDOF system. Because $\zeta = 5\%$, the damping force can be ignored, and the maximum acceleration that the SDOF can experience (a_{max}) is expressed as follows:

$$a_{\text{max}} = \frac{f_{r,\text{max}}}{m}, \tag{4.2}$$

where $f_{r,\text{max}}$ is the maximum restoring force. For the highest experienced ductility of 14 (Figure 4.12) and strain hardening of 1%,

$$f_{r,\text{max}} = F_y + \frac{F_y}{\delta_y} \times 0.01 \times (14\delta_y - \delta_y) = 1.13F_y = 0.23W, \tag{4.3}$$

resulting in $a_{\text{max}} = 0.23g$, which may further slightly increase because of the damping force.

The TCN model was not able to capture this cap with 83 motions in the training set. Instead of increasing the number of motions in the training set, e.g., by an order of magnitude, one possible solution to overcome this limitation is the use of Physics-informed Neural Networks (PINNs) [20, 8], which received increased attention in recent years. A PINN-based architecture can be thought of as a hybrid modeling approach, which combines the advantages of physics-based and data-driven approaches. The main advantage of a PINN is the ability to use physics-based information to complement the data-driven Artificial Intelligence (AI) model. This information is generally an important local information, e.g., the acceleration cap of the SDOF system, that requires a much larger number of training data compared to that needed for the AI model to learn global underlying physics. Using PINN, this acceleration cap can be introduced to the TCN model as a constraint, instead of expecting the TCN to learn the presence of this cap using a very large training data set. The integration of PINN into the TCN model is especially important considering that the amount of data with inelastic behavior from instrumented structures is limited. The incorporation of PINNs to the TCN model for overcoming the issue of the acceleration cap is worth exploring in future studies.

In terms of damage assessment, CAV of response, particularly the changes in the slope of CAV time history, is one of the good indicators of damage, as discussed earlier. Because of the differences in the predicted and computed response, predicted and computed CAV time history did not match, however there is an almost perfect match between the predicted and computed CAV histories normalized by the maximum CAV for four of the test motions with high ductility (Figure 4.13). This is consistent with the observations that the pattern of the predicted acceleration matches the true response and the predicted acceleration captures the elongated period due to inelastic response.

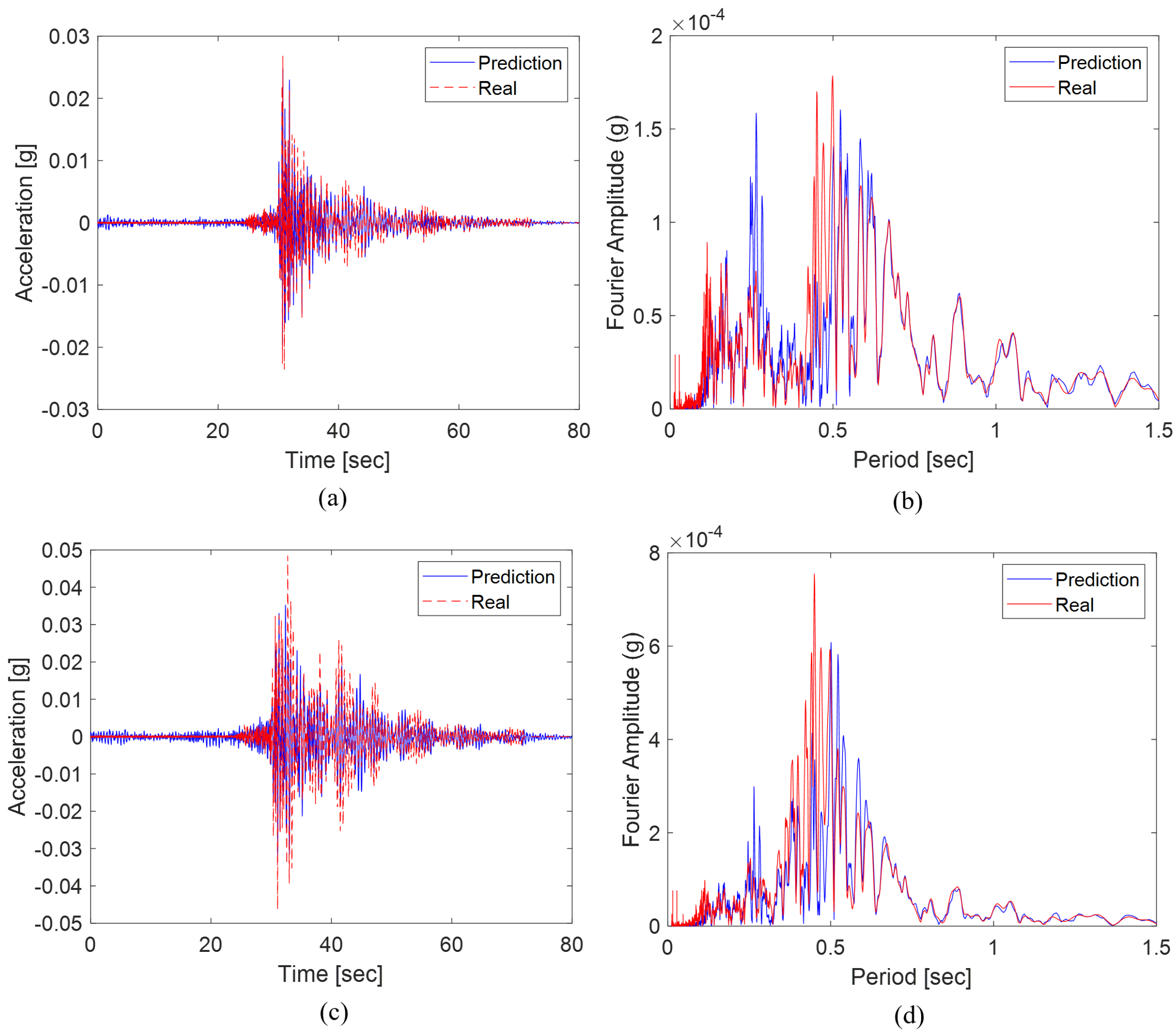

Figure 4.3: Comparison of predicted and recorded acceleration time history and the corresponding frequency contents in the NS direction of San Bernardino 6-story building at (a, b) 3rd floor, (c, d) 6th floor (Cabazon Earthquake of 08 May 2018).

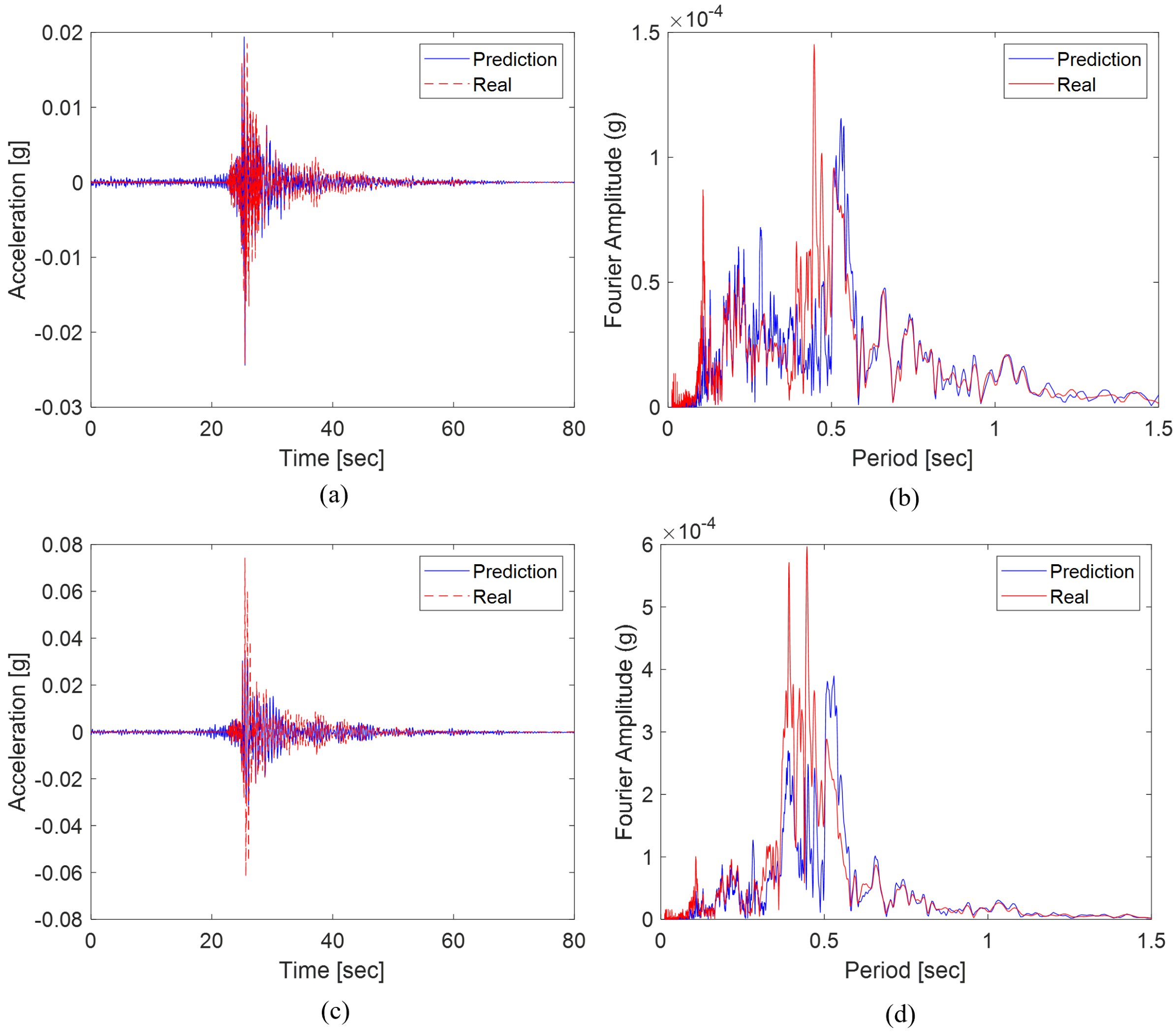

Figure 4.4: Comparison of predicted and recorded acceleration time history and the corresponding frequency contents in the NS direction of San Bernardino 6-story building at (a, b) 3rd floor, (c, d) 6th floor (Redlands Area Earthquake of 13 Feb. 2010).

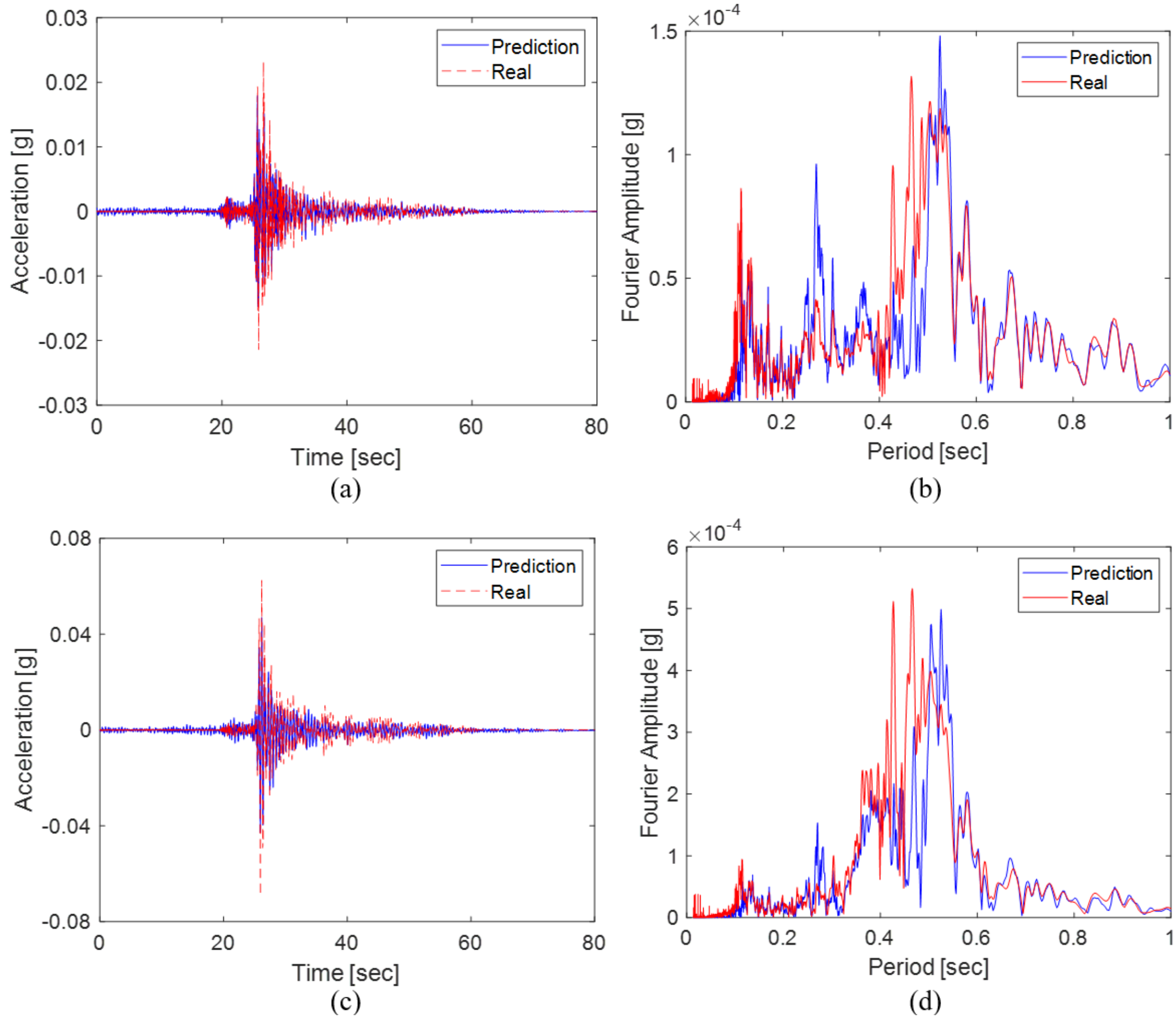

Figure 4.5: Comparison of predicted and recorded acceleration time history and the corresponding frequency contents in the NS direction of San Bernardino 6-story building at (a, b) 3rd floor, (c, d) 6th floor (Banning Earthquake of 06 Jan. 2016).

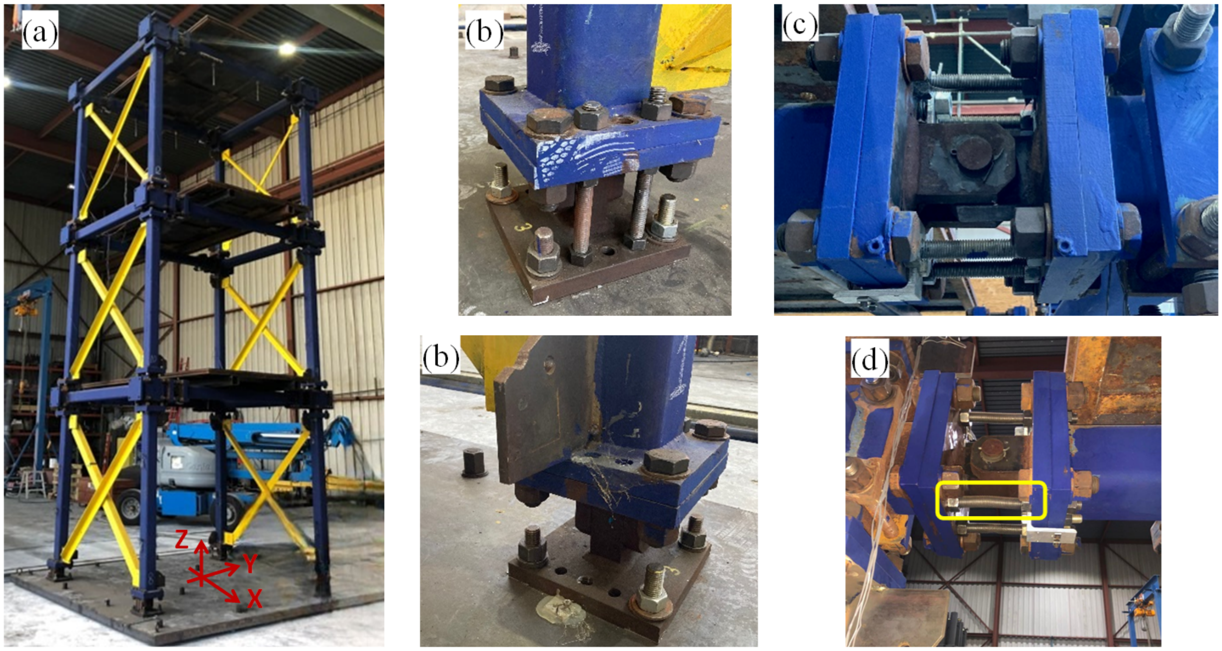

Figure 4.6: Structure tested on the shaking table: (a) overall setup, (b) two views of a column base, (c) end beam connection, and (d) inelastic response in the form of coupon buckling.

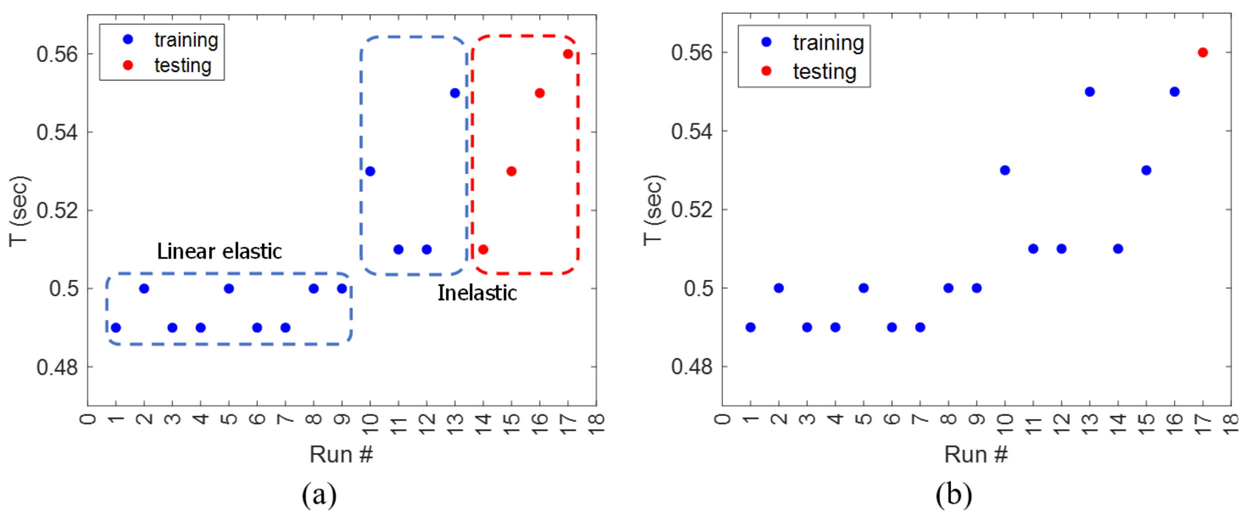

Figure 4.7: (a) First and (b) second training and testing sets used to predict the acceleration responses of the structure tested on the shaking table.

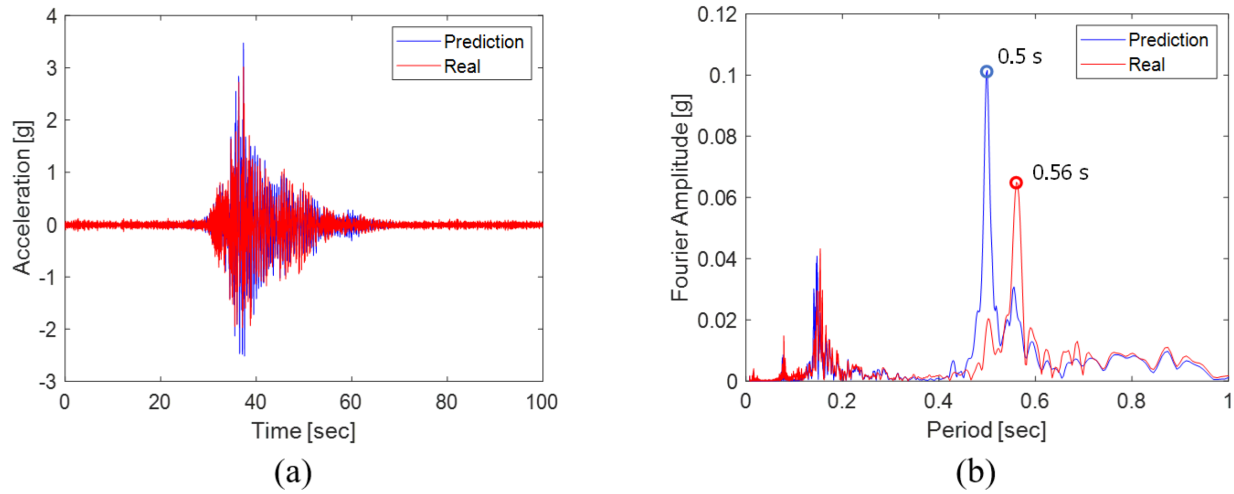

Figure 4.8: Comparison of (a) time history, (b) frequency content of predicted and recorded accelerations at 3rd floor of tested REPEAT frame (Run 17) [training set with 13 motions].

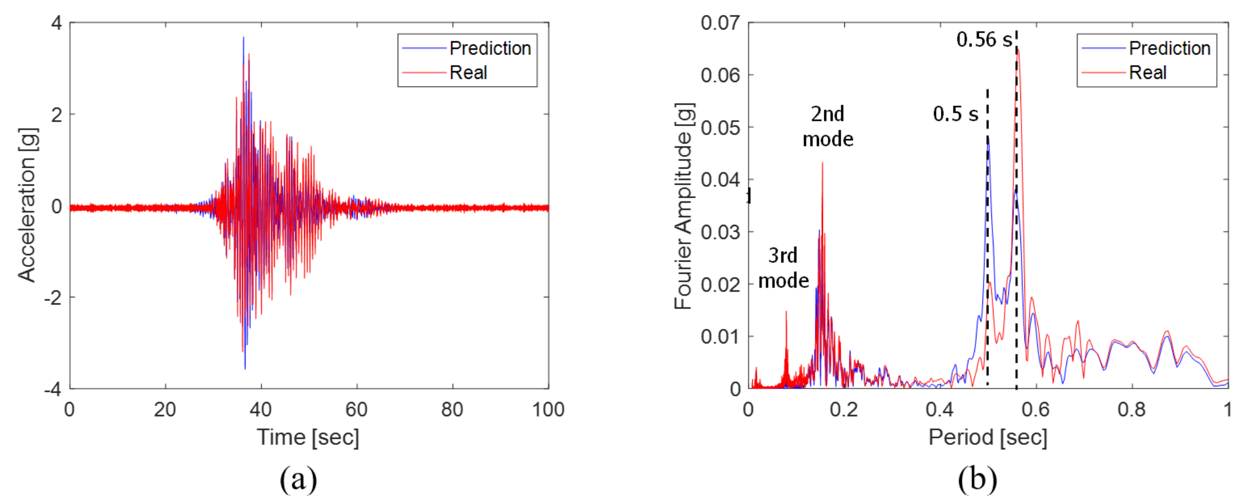

Figure 4.9: Comparison of (a) time history, (b) frequency content of predicted and recorded accelerations at 3rd floor of tested REPEAT frame (Run 17) [training set with 16 motions].

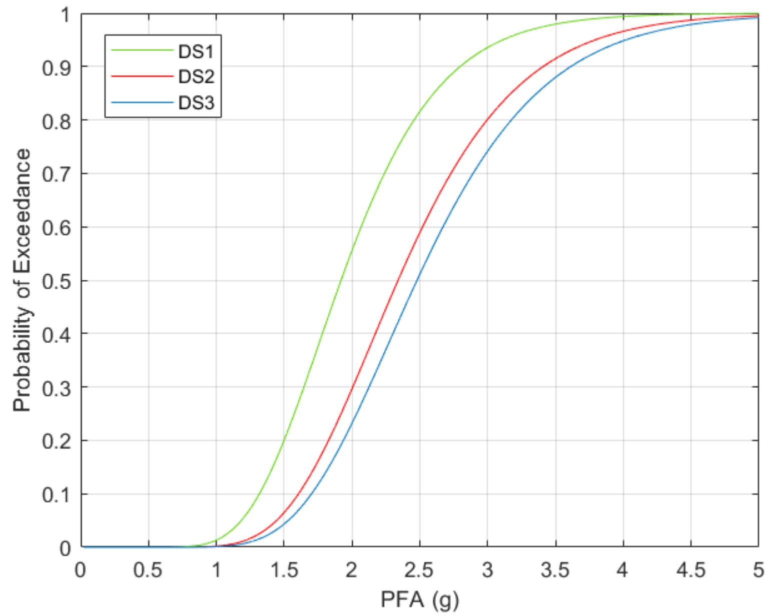

Figure 4.10: Fragility functions for the three damage states of a suspended ceiling.

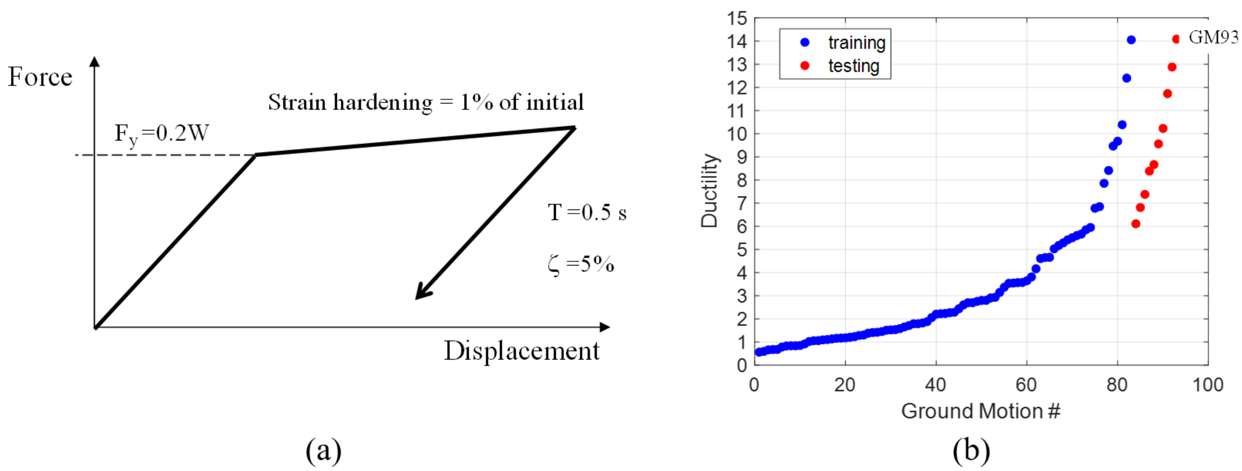

Figure 4.11: (a) Inelastic SDOF, (b) ductility demands of the motions in training and testing sets.

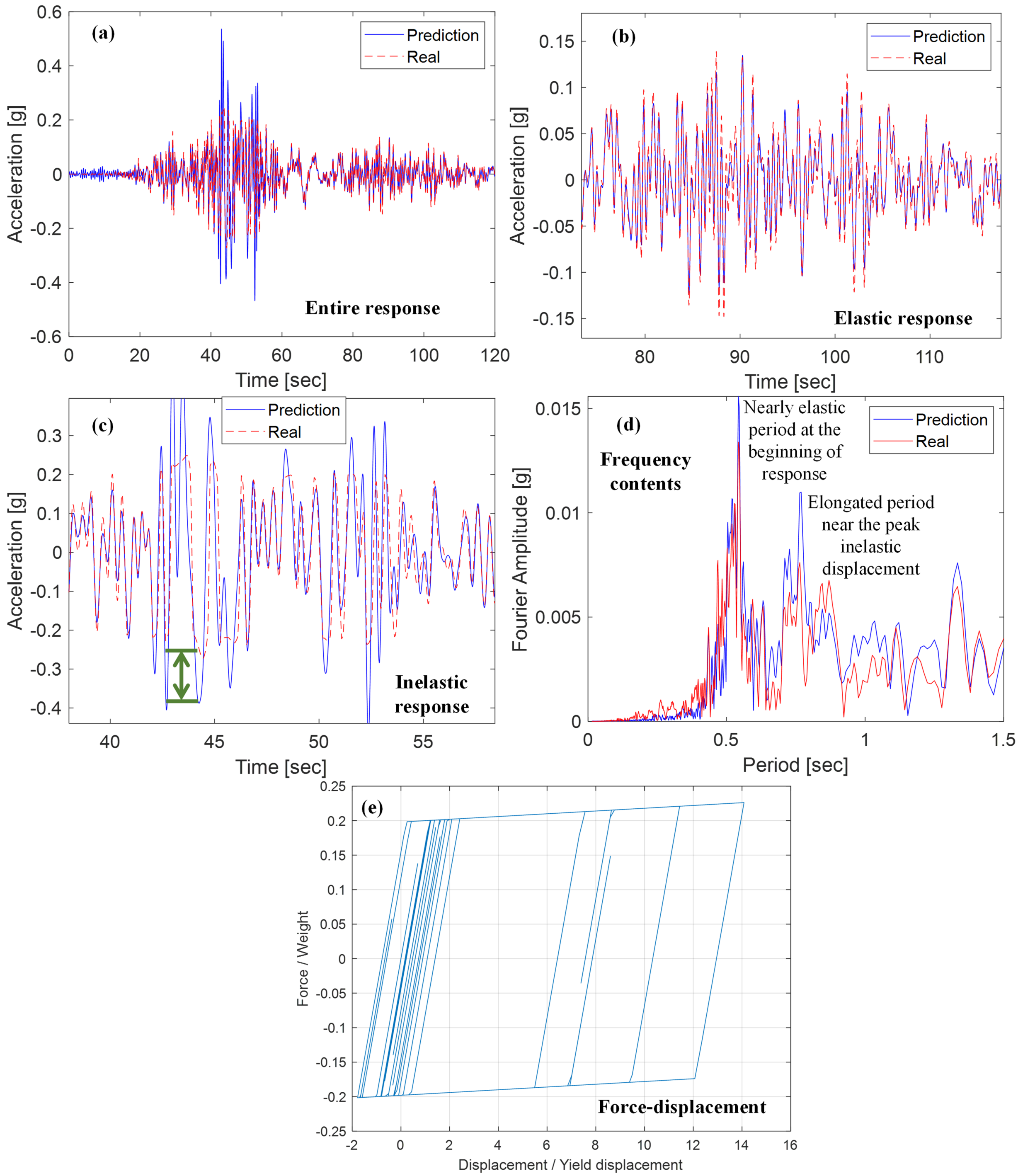

Figure 4.12: Comparison of predicted and computed accelerations of the inelastic SDOF for GM93: (a) entire response, (b) elastic response, (c) inelastic response, (d) frequency domain, (e) computed force-displacement relationship.

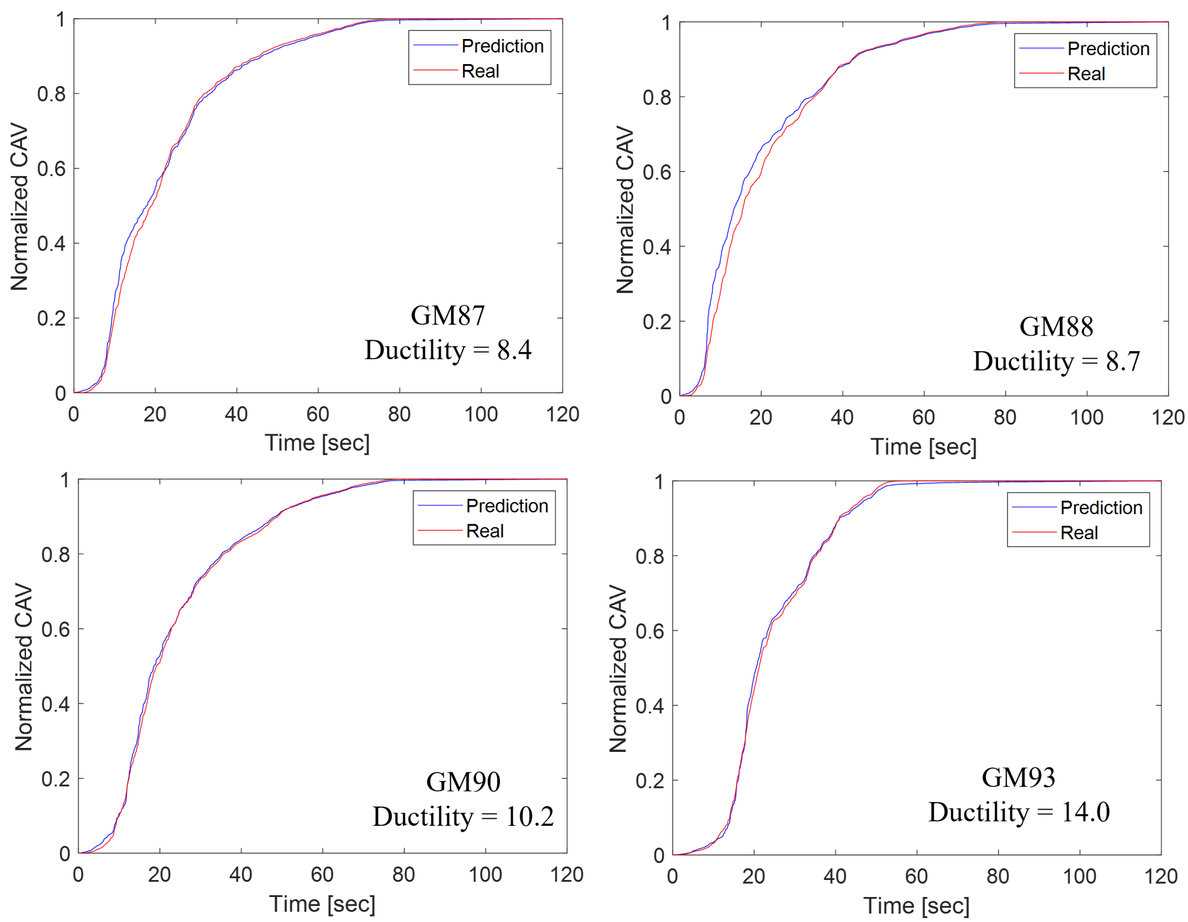

Figure 4.13: Normalized CAV time histories of four test motions with high ductility.

5 Ground Motion Reconstruction

The successful response predictions discussed in the earlier sections show that the TCN model can effectively capture the amplification function between the input ground motion and the output acceleration response. Because the ground motion can be calculated using the output acceleration response and the inverse of the amplification function, the TCN model is expected to perform well in reverse predictions using the inverse of the amplification function, given the accurate predictions in the forward case. With this expectation, ground motions are reconstructed from the recorded response accelerations using the TCN model in this section. The computation of the ground motion from the response is valuable in scenarios where ground motions are unavailable. It can facilitate the use of measured responses to obtain the ground motion and characterize the intensity of shaking in regions with scarce ground motion recording stations. In such locations, the number of conventionally instrumented buildings (e.g., those instrumented as part of CSMIP) is even lower. However, alternative instrumentation, such as the Community Seismic Network (CSN) [6] or apps like MyShake [11], which employ smartphone accelerometers and crowdsourcing, can be used. These alternative instruments at floor levels can predict ground motions at locations where ground motions are otherwise unavailable. Predicting ground motions also enables other benefits, such as facilitating the use of input-output methods for system identification, which are superior to output-only methods. Ground motions are reconstructed for the mid-rise and tall buildings discussed in earlier sections, and these predictions are detailed below.

5.1 6-STORY RC HOTEL BUILDING IN SAN BERNARDINO EW DIRECTION

In the earlier section focused on the prediction of floor accelerations of San Bernardino building in the EW direction, Channel 1 on the 1st floor was used as input, and Channel 4 on the 3rd floor was output. In the reverse case, to predict the ground motion, Channels 4 and 1 are used as input and output, respectively. The same 10 motions used for response predictions are used in the training set for ground motion predictions. Figure 5.1 compares the predicted and recorded ground motion acceleration history and the corresponding acceleration response spectra for two events in the testing set. It is observed that the time history and response spectra of the predicted accelerations match those of the recorded ones very well.

Ground motions are commonly characterized with several intensity measures (IMs) for various purposes, such as the development of ShakeMaps [21] and formulating the IM-based fragility functions for use in Performance-Based Earthquake Engineering (PBEE) [9]. Therefore,

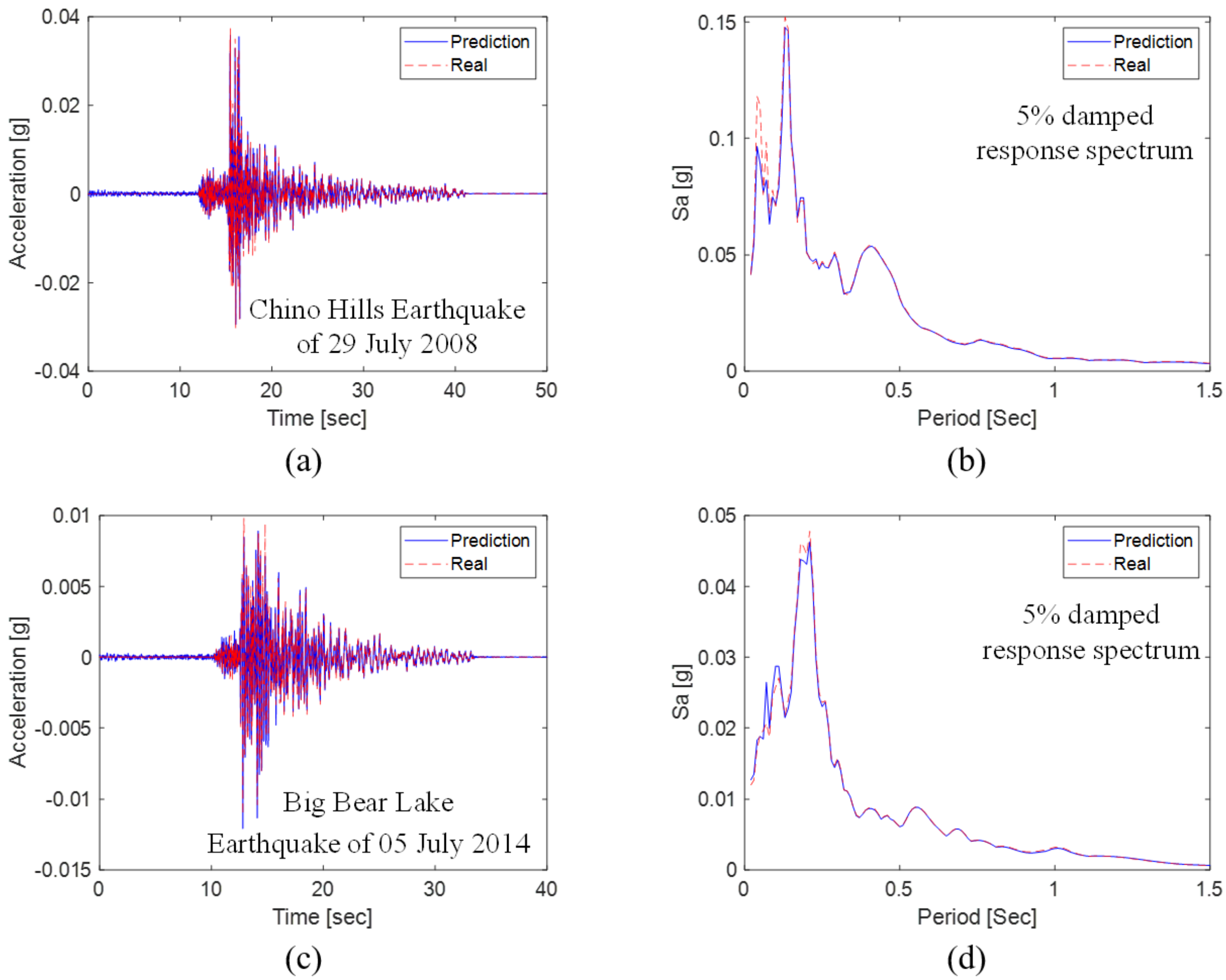

Figure 5.1: Identified periods of San Bernardino 6-story hotel building in (a) EW, and (b) NS directions in different earthquakes.

the various IMs of predicted and recorded ground motions, including Peak Ground Acceleration (PGA), spectral acceleration (S_a) at the 1st mode period, Arias Intensity (I_a), Peak Ground Velocity (PGV), and Cumulative Absolute Velocity (CAV), are compared for all motions in the testing set (Figure 5.2). The predicted values are very close to the recorded ones, showing that the developed TCN model is capable of predicting ground motions using the response accelerations of a mid-rise building.

5.2 TALL BUILDING WITH HIGHER MODES

The difficulty of predicting responses that include higher modes also applies to the ground motion reconstruction. Therefore, ground motions are predicted for the tall building in this section to evaluate the accuracy of the predictions. The same training and testing sets used for the response predictions are utilized for reconstructing the ground motions by changing the input and output

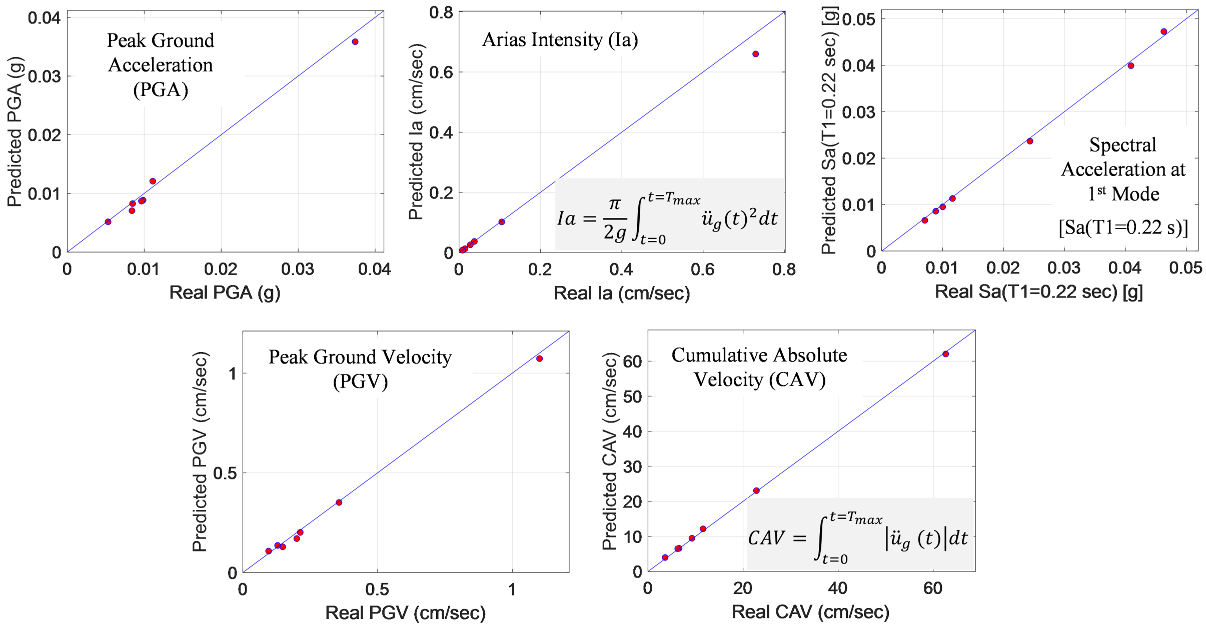

Figure 5.2: Identified periods of San Bernardino 6-story hotel building in (a) EW, and (b) NS directions in different earthquakes.

data. Three different ground motion predictions were performed using three training sets, where in all the sets, the output is the motion at the ground level, while the input in sets 1, 2, and 3 are the response accelerations at levels 46, 36, and 20, respectively. The presence of higher modes was expected in all three sets, but with different levels because of the mode shapes and the varying contribution of higher modes at different floors. As observed in Figure 5.3, the predicted ground motion time histories are close to the recorded ones, but not as close as the predictions for San Bernardino building with the first mode-dominated building response. These differences between the predictions and recorded ground motions are more clearly observed in the acceleration response spectra. Using observations from San Bernardino building and the tall building, it is concluded that ground motion predictions are accurate when the response is governed by the first mode, and more training data is needed for successful predictions involving higher modes or inelastic effects. However, it was not possible to explore how many more motions are needed in the training set for accurate predictions, because all the events recorded for this building are already used, and no additional data is available. This highlights the need for increased instrumentation of buildings and bridges.

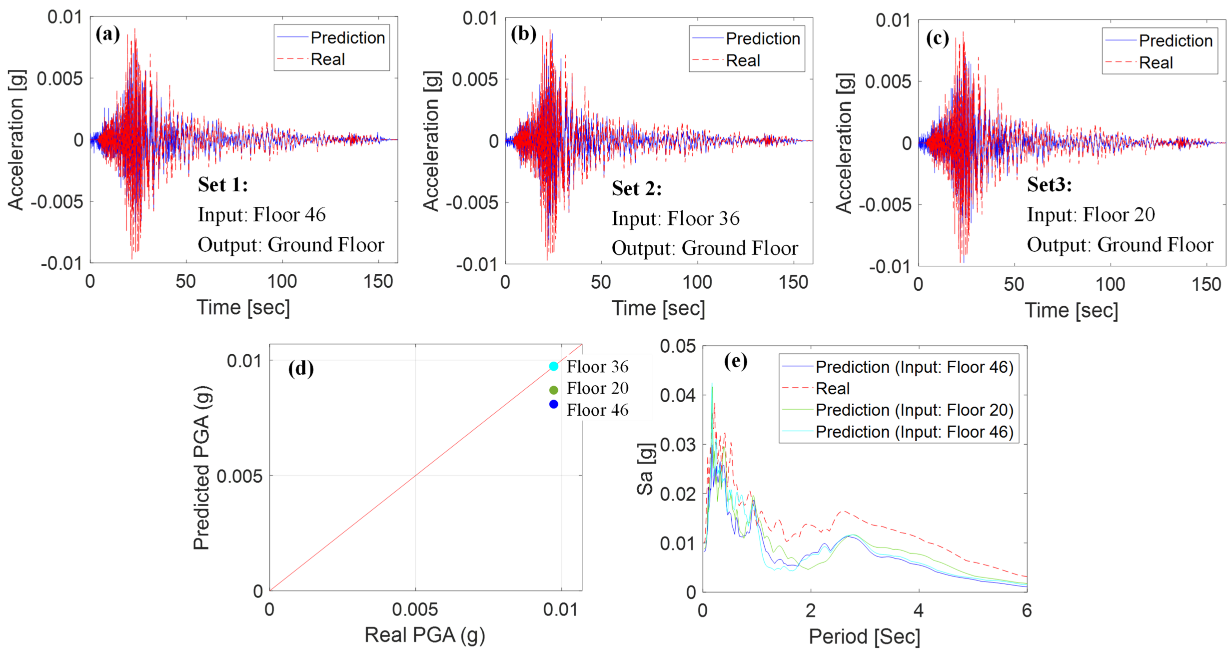

Figure 5.3: Comparison of predicted and recorded ground motion (a, b, c) acceleration time histories, (d) PGA, (e) 5% damped acceleration response spectra for the event in the testing set.

6 Results and Discussion

This chapter provides a summary of the results and conclusions and discusses them from different perspectives. To guide this discussion, Table 6.1 lists a summary of the TCN predictions for the studied structural systems.

Table 6.1: Features characterizing the earthquake response of different structural systems.

Prediction Type	System	$NM_{\textbf{training}}{}^{\star}$	Quality of Predictions
Linear elastic response	SDOF	10	Successful
	Low- & Mid-rise buildings	10	Successful
	Tall building	10	Successful
Inelastic response	Bilinear SDOF	83	Partially successful[†]
	Tested 3-story SMRF	13	Needs improvement
	Tested 3-story SMRF	16	Successful
	Mid-rise building	10	Needs improvement
	Mid-rise building	23	Successful
Ground motion	Mid-rise building	10	Successful
	Tall building	10	Successful[‡]

* $NM_{\text{training}} =$ # of motions in the training set
[†] PINNs is needed to improve peak response.
[‡] More data improves predictions.

6.1 INTERPRETATION OF RESULTS IN EARTHQUAKE ENGINEERING CONTEXT

The results of this study, achieved through the application of TCN, offer significant insights into structural response prediction and ground motion modeling in the context of earthquake engineering. The ability to predict both linear-elastic and inelastic responses with high accuracy provides a robust foundation for advancing performance-based earthquake engineering (PBEE) methodologies and enhancing structural health monitoring (SHM) practices.

6.1.1 Linear Elastic Response

The successful prediction of linear elastic responses across various building types highlights the effectiveness of TCN in capturing fundamental structural dynamics. For low-rise and mid-rise buildings, the TCN demonstrated its ability to model responses dominated by the first mode of vibration, accurately capturing the natural period and the varying damping ratio. Similarly, for tall buildings with higher modes, the TCN captured the influence of multiple modal frequencies and stiffness irregularities, such as those caused by transfer girders. Therefore, the TCN model was successful for systems that are characterized by not only relatively simple features, such as a numerical SDOF system characterized by a single natural period and damping ratio, but also those with more complex response such as a tall building with multiple modes of vibration contributing to the overall response. For these different systems, a training set size of 10 motions was sufficient for predicting the response. These results demonstrate the effectiveness of the TCN model even for structures with limited amount of data and underscore the potential of TCNs as a computationally efficient alternative to conventional numerical methods, reducing the reliance on time-intensive simulations while maintaining accuracy.

The predicted and true responses from multiple test motions, along with relevant fragility functions, were used to compute the probability of damage of a cooling tower assumed to be located at the roof of the 6 story San Bernardino building. The resulting probability of damage was very close using the true and precited responses. This preliminary exercise provided confidence in the model predicted responses to detect nonstructural (and structural) damage. To demonstrate the importance of predicting the entire time history, Cumulative Absolute Velocity (CAV), a parameter closely correlated to damage, was computed using the predicted and true responses of the same building and the resulting CAV time histories were very close to each other.

6.1.2 Nonlinear Response and Inelastic Behavior

The inelastic response predictions demonstrated that accurate predictions of inelastic response are possible with increased number of data in the training data set. The predictions in the NS direction of the 6-story building in San Bernardino demonstrated that the TCN model can capture response that cannot be conveniently obtained using state of the practice numerical models and dynamic analyses. Results of the 3-story structure tested on the shaking table highlighted that the developed TCN model can successfully predict the inelastic response beyond the inelastic response range employed in the training data set. For these two cases, the number of motions in the training set for accurate predictions was greater than those needed for the linear elastic response, however it was still a manageable number and less than 25 in both cases. The TCN model was successful in capturing the pattern of highly inelastic response in the case of the inelastic SDOF system, as well as the frequency contents of the response and the period elongation, however it could not capture the peak acceleration limited by the force capacity despite the use of a large number of motions in the training set. This highlighted the need to incorporate physical constrains in the methodology to increase accuracy and effectiveness. Overall, these three case studies demonstrated the efficacy and unique benefits of the TCN model in predicting different levels of inelastic response.

6.1.3 Ground Motion Predictions

In regions with sparse ground motion recording stations but structural response data widely available with alternative instrumentation, the ability of TCN to predict ground motions using structural response has significant implications for seismic hazard assessment. This capability enhances the accuracy of regional hazard maps and supports the development of site-specific ground motion models, particularly in the near-fault regions, where ground motion data from large magnitude earthquakes are lacking .

6.1.4 Implications for Earthquake Engineering Practice

The interpretation of results in the context of earthquake engineering highlights the transformative potential of TCN. A major broader impact of the developed TCN model is the ability to facilitate the prediction of the response of an instrumented building in future earthquakes without a structural analysis model. This ability provides a major advantage that maximizes accuracy and efficiency, compared to a conventional seismic assessment and performance prediction that is based on (i) developing the structural analysis model, and (ii) obtaining the structural response from either detailed but computationally extensive and demanding nonlinear time history analysis or computationally manageable but approximate linear dynamic or nonlinear static methods, as described in standards like [2].

As another impact, the accuracy and efficiency of TCN-based predictions can reduce uncertainties associated with traditional modeling approaches and improve the reliability of structural performance evaluations. The ability to model both elastic and inelastic responses across diverse structures provides engineers with a versatile tool for assessing seismic risk and designing resilient structures. Finally, the integration of ground motion and structural response predictions within a unified TCN framework streamlines the workflow for seismic hazard analysis and performance-based design.

Despite these advancements, the study also reveals the importance of comprehensive training datasets and the need for integrating physical constraints into data-driven models. Future research should focus on hybrid approaches, such as combining TCN with Physics-Informed Neural Networks (PINNs), to achieve accurate predictions with reasonable training data sizes and further enhance model interpretability and generalizability. By addressing these challenges, the application of TCN in earthquake engineering can be expanded.

6.2 COMPARATIVE ANALYSIS ACROSS CASE STUDIES

The application of TCN to various structural systems and scenarios in this study demonstrates their versatility and accuracy in predicting both linear and nonlinear responses. This section provides a comparative analysis of key findings across the case studies, highlighting the model's performance and limitations in different contexts.

6.2.1 Low-Rise and Mid-Rise Buildings

For low-rise and mid-rise buildings, such as San Bernardino 6-story RC hotel and Hemet 4-story RC hospital, the TCN successfully captured the dominant first-mode behavior of these structures. In the east-west (EW) direction of San Bernardino building, where the response remained linear elastic, the TCN achieved high correlation coefficients (0.91) between predicted and recorded responses. Similarly, for Hemet hospital building, predictions were accurate across a range of motions, demonstrating the model's ability to generalize within this building category.

The consistent accuracy in these cases indicates that TCN is well-suited for predicting responses dominated by single-mode behavior, with minimal complexity introduced by higher modes or inelastic effects. This makes the TCN a computationally efficient alternative to conventional methods for low- to mid-rise structures.

6.2.2 Tall Buildings with Higher Modes

The prediction of responses in tall buildings, such as the 54-story SMRF in Los Angeles, highlighted the TCN's ability to handle higher-mode effects and stiffness irregularities. For motions recorded in the north-south (NS) direction, the TCN successfully replicated the localized acceleration peaks observed at floors with transfer girders. While the model demonstrated strong agreement with recorded responses in both time and frequency domains, the complexity introduced by higher modes generally requires a more extensive training dataset to achieve comparable accuracy.

The comparison with low- and mid-rise buildings reveals that while TCNs perform robustly in these cases, the presence of higher modes in tall buildings necessitates careful dataset preparation. This includes ensuring sufficient representation of motions that excite multiple modes and any additional response introduced by structural irregularities.

6.2.3 Nonlinear Responses and Inelastic Behavior

In nonlinear response scenarios, such as San Bernardino building's north-south (NS) direction and the laboratory-tested REPEAT frame, the TCN captured critical phenomena like period elongation. For San Bernardino building, the TCN accurately predicted progressive period elongation due to stiffness degradation, aligning with physical observations of cracking and foundation rocking. Similarly, for the REPEAT frame, the model replicated both time-history responses and frequency-domain effects for tests with moderate inelasticity.

When compared to linear elastic cases, the nonlinear response predictions highlight the importance of diverse and representative training datasets. Inelastic responses are more challenging to predict due to their dependence on damage mechanisms and material properties, requiring comprehensive data to train the model effectively.

6.2.4 Observations and Insights

The comparative analysis across these case studies provides several key insights. The TCN framework consistently demonstrates high accuracy for linear elastic responses across various building types, particularly for low-rise and mid-rise structures. For tall buildings and nonlinear responses, the model's accuracy is significantly influenced by the diversity and representativeness of the training dataset, underscoring the importance of comprehensive data preparation. Additionally, the ability of the TCN to predict ground motions in sparsely instrumented regions highlights its potential to extend beyond structural response analysis, offering a valuable tool for seismic hazard assessment.

These findings highlight the flexibility and precision of the TCN framework across a range of applications. They also underscore areas for improvement, such as integrating hybrid modeling approaches and expanding datasets, to further enhance its performance. The adaptability of TCNs positions them as a promising tool for advancing earthquake engineering practices and strengthening the resilience of the built environment.

7 Conclusions, Limitations, and Future Work

The advancements presented in this study demonstrate the transformative potential of Temporal Convolutional Networks (TCNs) in efficiently and accurately predicting structural responses and ground motions. However, like any emerging methodology, the TCN framework has its constraints and areas for further enhancement. A critical assessment of the challenges encountered during the development and application of TCNs provides a roadmap for future research and underscores opportunities for integrating complementary approaches, such as Physics-Informed Neural Networks (PINNs), to address these limitations.

This chapter highlights the conclusions, primary limitations encountered, focusing on data constraints, model generalizability, and computational challenges. It also explores potential avenues for advancing the presented framework using PINNS, emphasizing interdisciplinary strategies to expand its applicability in earthquake engineering and beyond.

7.1 CONCLUSIONS

This study demonstrated the efficacy of TCN in predicting structural responses and ground motions, offering a robust and computationally efficient alternative to traditional modeling techniques. The TCN framework successfully captured both linear elastic and nonlinear inelastic behaviors across a diverse set of case studies, including low-rise, mid-rise, and tall buildings, as well as laboratory-tested frames. Additionally, the model effectively reconstructed ground motions in sparsely instrumented regions, addressing key challenges in seismic hazard assessment. Key contributions of this work include:

- A validated methodology for using TCN to predict time-history responses with high accuracy.
- Demonstration of the model's capability to handle complex phenomena, such as period elongation and higher-mode effects.
- Expansion of ground motion prediction techniques to under-instrumented areas, leveraging data from structural response.

While the results underscore the strengths of TCN, they also highlight limitations such as data constraints and the need for improved interpretability. Addressing these challenges through the integration of PINNs and enhanced training datasets could further advance the model's applicability.

In summary, the TCN framework represents a significant step forward in the application of machine learning to earthquake engineering. By combining computational efficiency with predictive accuracy, TCN holds the potential to transform performance-based earthquake engineering and structural health monitoring practices, ultimately contributing to safer and more resilient infrastructure in seismic regions.

7.2 LIMITATIONS: DATA CONSTRAINTS

The performance of TCN in predicting structural responses and ground motions is inherently tied to the quality and quantity of data used for training and validation. Despite the promising results demonstrated in this study, several data-related constraints were encountered, which highlight limitations in the current methodology and opportunities for improvement.

7.2.1 Scarcity of Inelastic Response Data

A significant constraint was the limited availability of inelastic response data from instrumented structures. Most existing datasets, such as those from CSMIP, primarily capture linear elastic responses during moderate seismic events. High-quality data for nonlinear responses, which involve phenomena such as period elongation, cracking, and stiffness degradation, are sparse due to the rarity of severe ground motions and the limited number of instrumented structures that experience such events.

To address this limitation, synthetic datasets generated from numerical simulations and laboratory tests were used to supplement real-world data. However, synthetic data often lack the complexity and variability of real-world conditions, which can introduce biases and reduce the generalizability of the TCN model.

7.2.2 Imbalance in Dataset Representation

Another key constraint was the imbalance in the dataset, with a disproportionate number of motions resulting in linear elastic response compared to those with nonlinear response. This imbalance affects the model's ability to generalize across different seismic intensity levels and structural behaviors. Although the TCN performed well for linear responses, its performance for nonlinear responses depended heavily on the inclusion of representative inelastic events in the training dataset.

7.2.3 Sparse Instrumentation in Key Regions

Sparse seismic instrumentation in certain geographic regions poses an additional challenge, particularly for ground motion prediction. While densely instrumented areas like urban California provide rich datasets, rural and underdeveloped regions often lack sufficient sensor coverage. This spatial disparity limits the applicability of the TCN model to regions with adequate data and highlights the need for extrapolation techniques to predict ground motions in sparsely instrumented areas.

7.2.4 Implications and Future Directions

Addressing these data constraints is critical for advancing the application of TCN in earthquake engineering. Future work should focus on expanding the availability of high-quality inelastic response data through enhanced instrumentation of structures in seismically active regions and the development of advanced numerical models that better replicate real-world conditions. Additionally, balancing datasets to include a wider range of seismic intensities and structural behaviors will improve the generalizability of the TCN framework. Integrating physics-informed constraints into the model could also help mitigate the impact of limited data by embedding domain knowledge directly into the learning process.

7.3 FUTURE WORK: PINNS

PINNs are an emerging class of machine learning models that integrate physical principles directly into the training process, ensuring that predictions adhere to established governing equations. By embedding domain knowledge, such as the equations of motion, into the loss function, PINNs can bridge the gap between purely data-driven models like TCN and traditional physics-based approaches. This integration offers a promising pathway to address some of the key limitations identified in this study.

7.3.1 Advantages of PINNs in Structural Response Prediction

The integration of PINNs into structural response prediction frameworks offers significant advantages over purely data-driven models. These advantages can be summarized as follows:

Reduced Data Dependency where PINNs utilize embedded physical constraints to guide the learning process, which reduces their reliance on extensive labeled datasets. This feature is particularly advantageous in situations where high-quality inelastic response data is limited, enabling PINNs to perform effectively even with constrained datasets.

Improved Generalization by integrating physical principles into the learning process where PINNs can generalize better to previously unseen scenarios, such as extreme ground motions or novel structural configurations. This ability to extrapolate beyond the training data makes PINNs more robust than purely data-driven models in handling diverse and challenging cases.

7.3.2 Potential Applications in Earthquake Engineering

The integration of PINNs into the TCN framework opens several avenues for advancing structural response and ground motion predictions:

Modeling Nonlinear Dynamics where PINNs can improve the modeling of inelastic responses by directly incorporating damage mechanics and material nonlinearities into the loss function. This capability allows for more accurate predictions of structural behaviors under extreme seismic events.

Ground Motion Prediction where in regions with sparse instrumentation, PINNs can combine physical models of wave propagation with limited observed data to enhance the accuracy of ground motion extrapolations. This approach provides a viable solution for seismic hazard assessment in under-monitored areas.

Multi-Scale Modeling where PINNs offer a unified framework for integrating both local phenomena, such as site-specific soil behavior, and global phenomena, such as structural responses. This multi-scale capability allows for comprehensive predictions that account for the complex interactions between soil-structure systems.

7.3.3 Challenges and Future Directions

Despite their advantages, the adoption of PINNs in earthquake engineering faces several challenges. Training PINNs often requires solving complex partial differential equations (PDEs), which can significantly increase computational costs compared to traditional neural networks. Additionally, ensuring numerical stability and convergence during training can be challenging, particularly for highly nonlinear systems.

Future research should explore hybrid models that combine the strengths of TCNs and PINNs. For example, a TCN could first predict an approximate response, which a PINN could refine by enforcing physical constraints. Developing efficient training algorithms for PINNs and integrating them into existing seismic analysis workflows will also be crucial for their widespread adoption.

7.3.4 Implications for Earthquake Engineering

The integration of PINNs into structural response prediction frameworks has the potential to revolutionize earthquake engineering. By combining the strengths of data-driven and physics-based approaches, PINNs offer a robust and interpretable solution for modeling complex nonlinear phenomena. This hybrid methodology aligns with the goals of performance-based earthquake engineering (PBEE) by improving the accuracy and reliability of structural assessments, even in data-scarce environments. As the field progresses, PINNs are likely to play a central role in advancing computational tools for seismic hazard analysis and structural health monitoring.

7.3.5 Application to Lifeline Infrastructure

The TCN framework can be adapted for critical lifeline systems such as bridges, pipelines, and electrical grids, which exhibit complex dynamic behavior during earthquakes. Predicting the response of these systems requires modeling interactions between multiple components and materials, an area where TCN can excel due to their ability to capture temporal dependencies.

7.3.6 Global Applications in Data-Scarce Regions

While this study focused on buildings in California, the TCN methodology can be extended to data-scarce regions worldwide. By leveraging global datasets and transfer learning techniques, TCNs can provide valuable predictions for regions with limited instrumentation, contributing to improved seismic resilience in underserved areas.

7.3.7 Beyond Earthquake Engineering

Beyond structural dynamics, TCN has potential applications in other domains where time-series analysis is critical. For example, they could be employed in wind engineering to predict aerodynamic responses of tall structures or in hydrology to model the dynamic effects of flooding on dams and levees. These extensions could benefit from the foundational developments made in this study.

REFERENCES

[1] ASCE. Minimum design loads and associated criteria for buildings and other structures. Technical Report ASCE/SEI 7-22, American Society of Civil Engineers, 2022.

[2] ASCE. Seismic evaluation and retrofit of existing buildings. Technical Report ASCE/SEI 41-23, American Society of Civil Engineers, 2023.

[3] J.M.W. Brownjohn, S.K. Au, Y. Zhu, Z. Sun, B. Li, J. Bassitt, E. Hudson, and H. Sun. Bayesian operational modal analysis of jiangyin yangtze river bridge. *Mechanical Systems and Signal Processing*, 110:210–230, 2018. URL: `https://doi.org/10.1016/j.ymssp.2018.03.027`.

[4] Y. Chen, Z. Sun, R. Zhang, L. Yao, and G. Wu. Attention mechanism based neural networks for structural post-earthquake damage state prediction and rapid fragility analysis. *Computers & Structures*, 281:107038, 2023. URL: `https://doi.org/10.1016/j.compstruc.2023.107038`.

[5] A.K. Chopra. *Dynamics of Structures, Theory and Applications to Earthquake Engineering*. Pearson Education, Hoboken, NJ, 5th edition, 2017.

[6] R.W. Clayton, T. Heaton, M. Kohler, M. Chandy, R. Guy, and J. Bunn. Community seismic network: A dense array to sense earthquake strong motion. *Seismological Research Letters*, 86(5):1354–1363, 2015. URL: `https://doi.org/10.1785/0220150094`.

[7] C. Cruz and E. Miranda. Evaluation of damping ratios for the seismic analysis of tall buildings. *Journal of Structural Engineering*, 143(1):04016144, 2017. URL: `https://doi.org/10.1061/(ASCE)ST.1943-541X.0001628`.

[8] S.S. Eshkevari, M. Takáč, S.N. Pakzad, and M. Jahani. Dynnet: Physics-based neural architecture design for nonlinear structural response modeling and prediction. *Engineering Structures*, 229:111582, 2021. URL: `https://doi.org/10.1016/j.engstruct.2020.111582`.

[9] S. Günay and K.M. Mosalam. Peer performance-based earthquake engineering methodology, revisited. *Journal of Earthquake Engineering*, 17(6):829–858, 2013. URL: `https://doi.org/10.1080/13632469.2013.787377`.

[10] Sepp Hochreiter and Jürgen Schmidhuber. Long short-term memory. *Neural Comput.*, 9(8):1735–1780, 1997. URL: `10.1162/neco.1997.9.8.1735`.

[11] Q. Kong, R.M. Allen, L. Schreier, and Y.W. Kwon. Myshake: A smartphone seismic network for earthquake early warning and beyond. *Science Advances*, 2(2):e150105, 2016. URL: `DOI:10.1126/sciadv.1501055`.

[12] A. Kundu and S. Chakraborty. *Deep learning-based metamodeling technique for nonlinear seismic response quantification*, volume 936, page 012042. IOP Publishing, September 2020.

[13] C. Lea, M.D. Flynn, R. Vidal, A. Reiter, and G.D. Hager. Temporal convolutional networks for action segmentation and detection. In *Proceedings of the IEEE Conference on Computer Vision and Pattern Recognition*, pages 156–165, 2017. URL: 10.1088/1757-899X/936/1/012042.

[14] B. Li and S.M. Spence. Metamodeling through deep learning of high-dimensional dynamic nonlinear systems driven by general stochastic excitation. *Journal of Structural Engineering*, 148(11):04022186, 2022. URL: https://doi.org/10.1061/(ASCE)ST.1943-541X.0003499.

[15] D. McCallen, A. Pitarka, H. Tang, K.M. Mosalam, F. Petrone, S. Günay, and C. Perez. An open access simulated earthquake ground motion database for a m7 hayward fault earthquake in the san francisco bay region. *Earthquake Spectra*, In publication, 2025.

[16] Khalid M Mosalam and Yuqing Gao. *Artificial Intelligence in Vision-Based Structural Health Monitoring*. Springer Nature, Switzerland, 2024. URL: https://doi.org/10.1007/978-3-031-52407-3.

[17] S. Muin and K.M. Mosalam. Cumulative absolute velocity as a local damage indicator of instrumented structures. *Earthquake Spectra*, 33(2):641–664, 2017. URL: https://doi.org/10.1193/090416EQS142M.

[18] S. Muin and K.M. Mosalam. Localized damage detection of csmip instrumented buildings using cumulative absolute velocity: A machine learning approach. In *Proceedings of the SMIP18 Seminar on Utilization of Strong-Motion Data*, volume 25, Sacramento, CA, USA, 2018.

[19] Y.J. Park and A.H.S. Ang. Mechanistic seismic damage model for reinforced concrete. *Journal of Structural Engineering*, 111(4):722–739, 1985. URL: https://doi.org/10.1061/(ASCE)0733-9445(1985)111:4(722).

[20] M. Raissi, P. Perdikaris, and G.E. Karniadakis. Physics-informed neural networks: A deep learning framework for solving forward and inverse problems involving nonlinear partial differential equations. *Journal of Computational Physics*, 378:686–707, 2019. URL: https://doi.org/10.1016/j.jcp.2018.10.045.

[21] C.B. Worden, M. Hearne, and E.M. Thompson. Shakemap v4 software, 2018.

[22] Qingyu Zhang, Maozu Guo, Lingling Zhao, Yang Li, Xinxin Zhang, and Miao Han. Transformer-based structural seismic response prediction. *Structures*, 61:105929, 2024. URL: https://doi.org/10.1016/j.istruc.2024.105929.

[23] R. Zhang, Z. Chen, S. Chen, J. Zheng, O. Büyüköztürk, and H. Sun. Deep long short-term memory networks for nonlinear structural seismic response prediction. *Computers & Structures*, 220:55–68, 2019.

[24] K. Zhong, J.G. Navarro, S. Govindjee, and G.G. Deierlein. Surrogate modeling of structural seismic response using probabilistic learning on manifolds. *Earthquake Engineering & Structural Dynamics*, 52(8):2407–2428, 2023. URL: `https://doi.org/10.1002/eqe.3839`.

The Pacific Earthquake Engineering Research Center (PEER) is a multi-institutional research and education center with headquarters at the University of California, Berkeley. Investigators from over 20 universities, several consulting companies, and researchers at various state and federal government agencies contribute to research programs focused on performance-based earthquake engineering.

These research programs aim to identify and reduce the risks from major earthquakes to life safety and to the economy by including research in a wide variety of disciplines including structural and geotechnical engineering, geology/ seismology, lifelines, transportation, architecture, economics, risk management, and public policy.

PEER is supported by federal, state, local, and regional agencies, together with industry partners.

PEER Core Institutions

University of California, Berkeley (Lead Institution)
California Institute of Technology
Oregon State University
Stanford University
University of California, Davis
University of California, Irvine
University of California, Los Angeles
University of California, San Diego
University of Nevada, Reno
University of Southern California
University of Washington

Pacific Earthquake Engineering Research Center
University of California, Berkeley
325 Davis Hall, Mail Code 1792
Berkeley, CA 94720-1792
Tel: 510-642-3437
Email: peer_center@berkeley.edu

ISSN 2770-8314
https://doi.org/10.55461/IPOS1888